DOI: 10.1002/adem.201080131

A Parametrical Analysis on the Elastic Anisotropy of Woven Hierarchical Tissues**

By *Qiang Chen* and *Nicola M. Pugno**

In this paper, the elastic properties of 2-D woven hierarchical tissues are modeled, considering matrix transformation and stiffness averaging, assuming the warp and fill yarns (level 0) an orthotropic material. The tissue at level 1 is considered as the fabric composed of warp and fill yarns at level 0. Warp and fill yarns at level 1 are defined as ''pieces'' of such 1-level tissue and have a different mismatch between the inclination of their longitudinal axes and those of the composing sub-fibers. Similarly, based on warp and fill yarns at level 1, we generate warp and fill yarns at level 2 and thus tissues with two hierarchical levels, and so on. We compare our theory with experiments on tendons from the literature and on leaves performed by ourselves. The result shows the possibility of designing a new class of hierarchical 2-D scaffolds by tailoring the elastic anisotropy, better matching the anisotropy of the biological tissues and thus maximizing their regeneration at each hierarchical level.

Tissue engineering seeks to repair or regenerate tissues through combinations of implanted cells, biomaterial scaffolds and biologically active molecules. The rapid restoration of tissue biomechanical function needs to replicate structural and mechanical properties using novel scaffold design.[1] The structure of a tissue may be described at several levels, with dimensions ranging from nano-scale to macro-scale, e.g., in describing a tendon, there are several distinctive levels from collagen molecule to the tendon itself.[2,3] Many soft biological or artificial tissues exhibit the anisotropic, inhomogeneous, and nonlinear mechanical behaviors,[4–7] because of the random orientation and mechanical properties of collagen molecule, e.g., the heart valve tissue.[8]

Accordingly, many contributions are today devoted to create bio-scaffolds with varieties of structures in order to match the structural and mechanical properties of natural tissues, a key requirement to maximize the tissue regeneration; moreover, a broad range of fabrication technologies are employed from earlier textile technologies to computational topology design and solid free-form fabrication.[9–11] Even so, the structural hierarchy is still difficult to be produced, or if some hierarchical structures can be developed, they are not controllable. In this regard, it seems that a little success has been achieved. Moutos *et al*.[1] developed a three-dimensional woven composite scaffold with the proper anisotropy for cartilage tissue engineering; experimental results showed that the mechanical properties are comparable to those of the native articular cartilage.

Moreover, recent literature focuses on multiscale modeling of biological materials in physiological and disease states,[12] and specifically on applications to collagenous tissues such as bone and others.[13] Especially, Buehler and his group[14,15] studied the collagen molecule and fibril by molecular simulations. They explained how nature can build a strong hierarchical structure by using weak materials.[16,17]

Differently from other multiscale models, based on self-similar or quasi-self-similar statistics,[4,18] we here consider a fully deterministic approach. The intrinsic material properties appearing at the zero level in our woven fabric hierarchical model could be *ab-initio* derived from fully atomistic simulations, as successfully done by Tang *et al*.[19] for nonwoven hierarchical composites.

Tendons are typical hierarchical biological structures. They have five hierarchical levels, ranging from the collagen molecule, collagen fibril, collagen fiber, fascicle, and the tendon itself, see Figure 1.[20] The mechanical properties of the first three levels were investigated by Yang[21] basing on atomic force microscopy (AFM). Sasaki and Odajima[22,23] and Bozec and

[*] *Prof. N. M. Pugno, Dr. Q. Chen*
Laboratory of Bio-Inspired Nanomechanics ''Giuseppe Maria Pugno'', Department of Structural Engineering and Geotechnics, Politecnico di Torino, Torino, 10129, (Italy)
E-mail: nicola.pugno@polito.it

[**] *Nicola M. Pugno is supported by Regione Piemonte, METREGEN (2009–2012) ''Metrology on a cellular and macromolecular scale for regenerative medicine''. The authors wish to thank Luca Boarino of NanoFacility Piemonte, INRiM, a laboratory supported by the Compagnia di San Paolo, for the SEM images reported in Figure 2.*

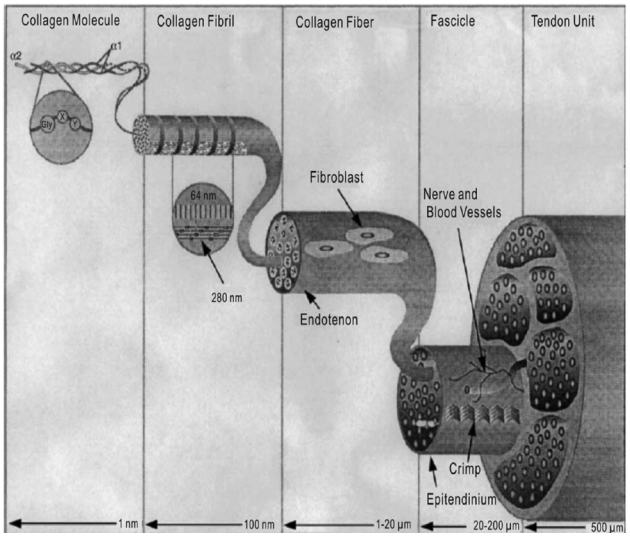

Fig. 1. Schematic of the structural hierarchy in tendons.[20]

Horton[24] investigated the mechanical properties of the single collagen molecule by X-ray diffraction technology and AFM: the former determined stress–strain relationship and estimated the longitudinal Young's modulus of the collagen molecule; the later focused on the mechanical response of type I collagen monomer. Van der Rijt *et al*.[25] measured the Young's modulus of the single fibril in ambient conditions and in aqueous media by AFM,[26] using scanning mode bending tests performed with an AFM, and they gave the bending moduli of single electrospun type I collagen fibers, at ambient conditions or in phosphate-buffered saline. As for the collagen fascicles, Yin and Elliott[27] built a transversely isotropic biphasic mixture model and studied the viscoelastic properties of collagen fascicles from mouse tail tendons; also Young's moduli and Poisson's ratios were reported.

Leaf is another example of hierarchical biological material. Due to its interesting mechanical properties (for instance, tensile strength and elastic modulus), plant fibers have been used in some composite materials. Some papers[28–31] about mechanical properties of pineapple leaf fibers and sisal fibers and their related bio-composites have contributed to this topic.

In this paper, a two-dimensional hierarchical woven tissues, treated with the methods of continuum mechanics and the stiffness averaging, are investigated in order to design tissues with desired anisotropic elasticity. In particular, the anisotropy of the tissue is controllable by changing the angle between fill and warp yarns and/or the volumetric fractions of fibers at different hierarchical levels. Experimental results on tendons from the literature and leaves performed by authors are compared with the theoretical predictions. We investigate here the hierarchical properties of the Aechmea aquilegia, which is modeled with three hierarchical levels, according to observations of the cross sections that we made with a scanning electron microscope (SEM; Fig. 2).

This paper is organized into seven sections: after this Introduction, Section 2 presents the theory which is used in the design of tissues. The formulas of elastic properties for general hierarchical tissues are derived in Section 3. In Section 4, two kinds of self-similar structures are introduced and investigated in detail, and parametric analyses are performed for different orientation angles and different relative volumetric ratios of warp to fill yarns. In Section 5, the comparison between theoretical predictions and experimental results from the literature on tendons is shown. In Section 6, experiments on the Aechmea aquilegia leaf that we carried out are described and compared with our hierarchical theory. Finally, concluding remarks are made in Section 7.

Matrix Transformation and Stiffness Averaging

In this section, two fundamental methods that we use to model hierarchical tissues, i.e., matrix transformation and stiffness averaging, are illustrated.

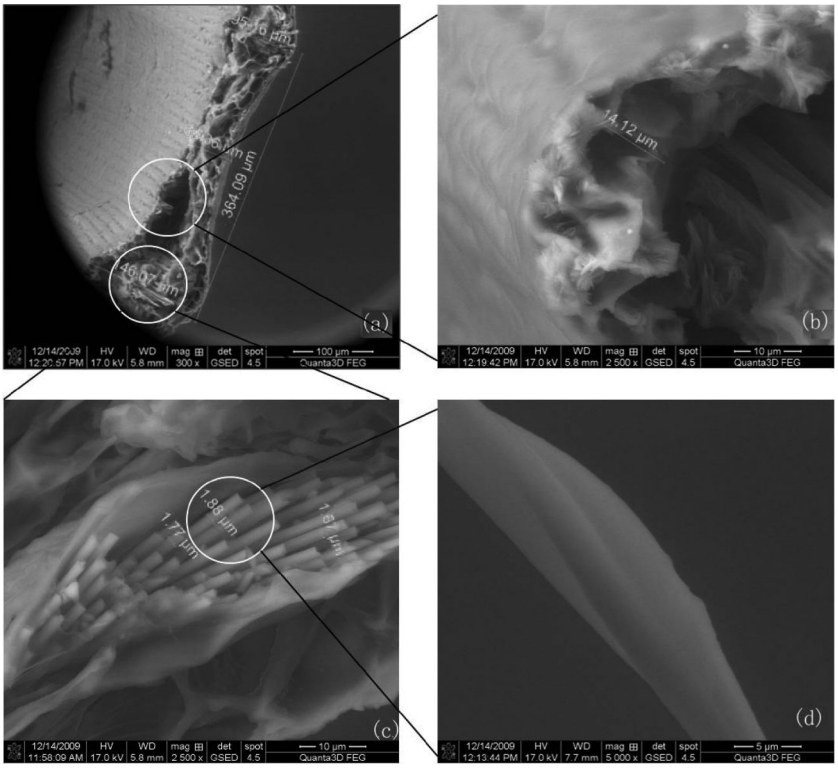

Fig. 2. The structural hierarchy of the Aechmea aquilegia leaf sample under SEM. (a): leaf; (b): matrix; (c): fiber bundle; and (d): single fiber.

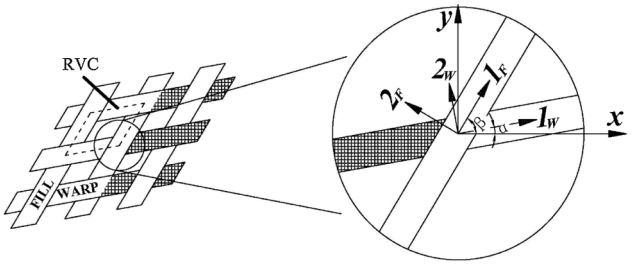

Fig. 3. Schematic of the woven structure.

It is well known in the mechanics of composites[32] that the stiffness matrix of composite structures can be obtained by linear volumetric averaging only for particular cases, including the case of plane reinforcement composites. Since our theory treats only the in-plane elastic behavior of the tissue, we adopt here, as done in previous papers,[33] the stiffening average method. The complexity of our model is in fact not due to out-of-plane configurations but rather to the considered hierarchical geometry. Other more sophisticated methods, such as the principle of equivalent homogeneity and polydisperse or three-phase model could also be invoked.

Two local coordinate systems ($1_W - 2_W$ for warp yarns and $1_F - 2_F$ for fill yarns) and a global coordinate system ($x - y$) are introduced (Fig. 3). Warp and fill yarns are assumed to be orthotropic. According to the coordinate system transformation matrix [T], in the global coordinate system, the stress–strain relationship of a single yarn (fill and warp) can be expressed by the stress tensor $\{\sigma_{ij}\}$and strain tensor $\{\varepsilon_{ij}\}$ as:[34]

$$\{\sigma_{ij}\} = [T]^{-1}\left\{\sigma^*_{ij}\right\} = [T]^{-1}[Q^*]\left\{\varepsilon^*_{ij}\right\} = [T]^{-1}[Q^*][T]\{\varepsilon_{ij}\} \quad (1)$$

where [Q^*] is the elastic matrix in the local coordinate system (*).

Then, the new elastic matrix [Q] in the global coordinate system can be expressed as a function of the fiber elastic properties and fiber orientation:

$$[Q] = [T]^{-1}[Q^*][T] \quad (2)$$

Thus, for example, for fill yarns, the relationship between the elastic matrices $[Q^*]_F$ and $[Q]_F$ is:

$$[Q]_F = [T(\beta)]^{-1}[Q^*]_F[T(\beta)] \quad (3)$$

[$T(\beta)$] is the transformation matrix for an orientation angle β made by the local coordinate axis 1_F and the global coordinate axis x (Fig. 3); the angle β is defined as a positive when it is counterclockwise.

For the two-dimensional case, the elastic matrix of fill yarns in local coordinate system is:

$$[Q^*]_F = \begin{pmatrix} Q^*_{11,F} & Q^*_{12,F} & 0 \\ Q^*_{21,F} & Q^*_{22,F} & 0 \\ 0 & 0 & 2Q^*_{66,F} \end{pmatrix} \quad (4)$$

where $Q^*_{ij,F}$ are components of the elastic matrix (4), which are defined as:

$$Q^*_{11,F} = \frac{E_{1,F}}{1-\mu_{12,F}\,\nu_{21,F}}, Q^*_{12,F} = \frac{\mu_{21,F}\,E_{1,F}}{1-\mu_{12,F}\,\mu_{21,F}},$$
$$Q^*_{22,F} = \frac{E_{2,F}}{1-\mu_{12,F}\,\mu_{21,F}}, Q^*_{66,F} = G_{12,F}$$

with $E_{i,F}$ Young's moduli, $\mu_{ij,F}$ Poisson's ratios, and $G_{ij,F}$ shear moduli, of fill yarns along the specified directions.

Thus, the elastic matrix of fill yarns in the global coordinate system is:

$$[Q]_F = \begin{pmatrix} Q_{11,F} & Q_{12,F} & 2Q_{16,F} \\ Q_{21,F} & Q_{22,F} & 2Q_{26,F} \\ Q_{61,F} & Q_{62,F} & 2Q_{66,F} \end{pmatrix} \quad (5)$$

The transformation matrix [$T(\beta)$] is:

$$[T(\beta)] = \begin{pmatrix} \cos^2\beta & \sin^2\beta & 2\cos\beta\sin\beta \\ \sin^2\beta & \cos^2\beta & -2\cos\beta\sin\beta \\ -\cos\beta\sin\beta & \cos\beta\sin\beta & \cos^2\beta - \sin^2\beta \end{pmatrix} \quad (6)$$

Substituting the subscript F with W, we can obtain the corresponding parameters for warp yarns. However, for warp yarns, the angle β in Equation 6 should be replaced by α, see Figure 3.

Note that the relationship: $[T(\beta)][T(\alpha)] = [T(\alpha+\beta)] = [T(\alpha)][T(\beta)]$ holds; moreover, when $\alpha+\beta = k\pi$, ($k = 0, \pm1, \pm2, \ldots$), [$T(\alpha)$] and [$T(\beta)$] are reciprocal.

If warp and fill yarns are treated as two different materials, then, based on the stiffness averaging method, we find the elastic matrix for woven structures[35]:

$$[Q] = \frac{V_F}{V_F+V_W+V_M}[Q]_F + \frac{V_W}{V_F+V_W+V_M}[Q]_W + \frac{V_M}{V_F+V_W+V_M}[Q]_M = v_F[Q]_F + v_W[Q]_W + (1-v_F-v_W)[Q]_M \quad (7)$$

in which we have assumed the presence of a filling matrix (subscript M), otherwise:

$$[Q] = \frac{V_F}{V_F+V_W+V_P}[Q]_F + \frac{V_W}{V_F+V_W+V_P}[Q]_W = v_F[Q]_F + v_W[Q]_W \quad (8)$$

V_F, V_W, V_M, and V_P are fill yarns, warp yarns, matrix, and pore volumes in a representative unit cell, respectively; v_F and v_W are fill and warp yarns' volumetric fractions, respectively.

Following Lee *et al.*[36] and extending their results of plain woven, the calculations of these volumetric fractions are given below. Firstly, two geometric arrangements are assumed[37]:

(1) The cross-sectional shape of yarns is assumed to be lenticular (Fig. 4).
(2) Yarns are incompressible and yarn to yarn distance between two overlaps is constant.

RESEARCH ARTICLE

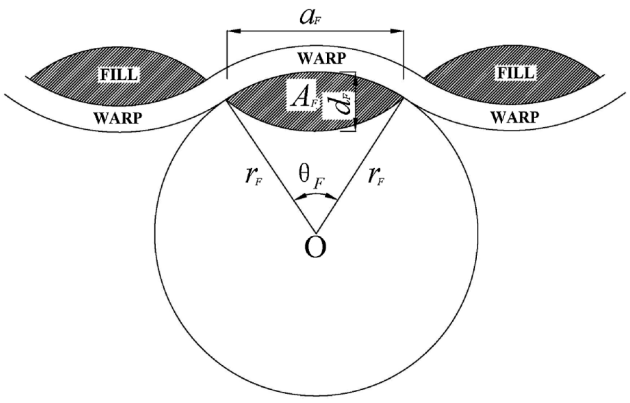

Fig. 4. Geometrical parameters of the fill yarn's cross-section.

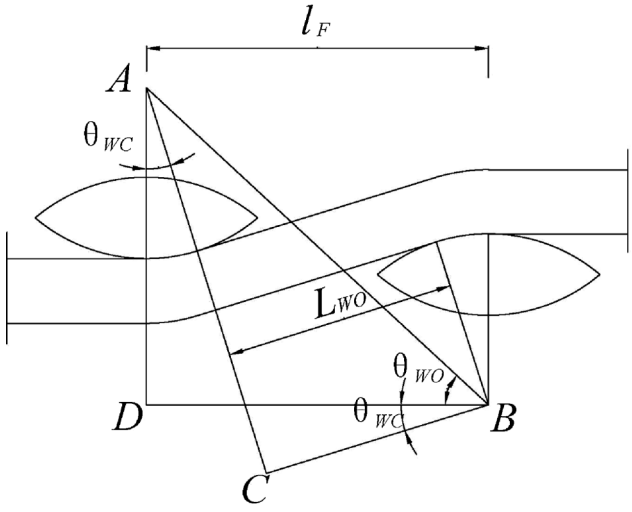

Fig. 5. Geometrical relationships between different parameters.

Based on the two assumptions, the main geometric parameters are expressed as follows (Fig. 4)[36]:

$$a_F = \frac{a_F^{90}}{\sin(\beta - \alpha)} \tag{9}$$

$$r_F = \frac{1}{4d_F}\left(d_F^2 + a_F^2\right) \tag{10}$$

$$\theta_F = 2\sin^{-1}\left(\frac{2a_F d_F}{d_F^2 + a_F^2}\right) \tag{11}$$

$$A_F = r_F^2(\theta_F - \sin\theta_F) \tag{12}$$

where a_F^{90} denotes fill yarn width when fill and warp yarns are perpendicular to each other, a_F and d_F are its width and thickness, respectively; r_F, θ_F, and A_F are radius, central angle, and cross-sectional area of fill yarns, see Figure 4.

The subscript F denotes fill yarns and can be replaced by the subscript W to treat warp yarns; thus, geometric parameters of warp yarns are expressed similarly.

According to a simple geometric analysis, the lengths of the segments AD and AC in Figure 5 are expressed as:

$$\overline{AD} = 2r_F + d_W - d_F;\ \overline{AC} = 2r_F + d_W \tag{13}$$

With the above outcomes, the length of the segment AB can be obtained $\left(l_F = \overline{DB}\right)$ as:

$$\overline{AB} = \sqrt{l_F^2 + (2r_F + d_w - d_F)^2} \tag{14}$$

thus, the ''crimp angle'' θ_{WC}, see Figure 5, is calculated as:

$$\begin{aligned}\theta_{WC} &= (\theta_{WO} + \theta_{WC}) - \theta_{WO} \\ &= \sin^{-1}\left(\frac{2r_F + d_W}{\sqrt{l_F{}^2 + (2r_F + d_W - d_F)^2}}\right) \\ &\times -\sin^{-1}\left(\frac{2r_F + d_W - d_F}{\sqrt{l_F{}^2 + (2r_F + d_W - d_F)^2}}\right)\end{aligned} \tag{15}$$

where, θ_{WO} is defined in Figure 5.

Then, formulas used to calculate the crimp, oblique, and horizontal lengths of single warp yarn in a representative unit cell are respectively found as:

$$L_{WC} = \theta_{WC}(2r_F + d_W) \tag{16}$$

$$L_{WO} = \sqrt{l_F{}^2 - 2d_F(2r_F + d_W) + d_F{}^2} \tag{17}$$

$$L_{WH} = 0 \tag{18}$$

Likewise, we can get similar results in the fill direction by substituting the subscript W with F. Thus, V_W and V_F can be determined.

For the generalized textile (Fig. 6), we similarly find:

$$\begin{aligned}V_U &= (d_F + d_W)(s + t - 1)l_F(p + q - 1)l_W \\ V_W &= (p + q - 1)A_W(L_{WC} + L_{WO} + L_{WH}) = N_W A_W L_W \\ V_F &= (s + t - 1)A_F(L_{FC} + L_{FO} + L_{FH}) = N_F A_F L_F \\ V_P &= V_U - V_W - V_F\end{aligned} \tag{19}$$

$$v_W = \frac{V_W}{V_W + V_F + V_P} = \frac{V_W}{V_U};\ v_F = \frac{V_F}{V_W + V_F + V_P} = \frac{V_F}{V_U} \tag{20}$$

where N_W and N_F are the total numbers of warp and fill yarns in the representative unit cell; L_W and L_F are the lengths of warp and fill yarns, respectively, in the representative unit cell. Also, it is worth noting that L_{WC} and L_{WO} are identical to those calculated by Equations 16 and 17; however, L_{WH} and

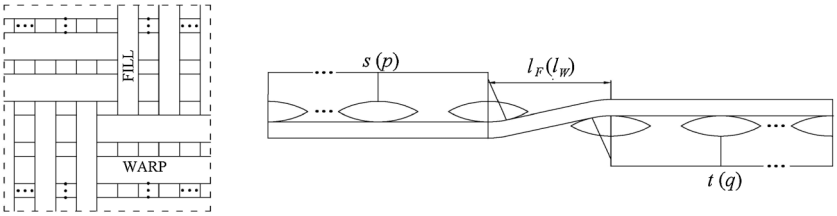

Fig. 6. Schematics of a generalized woven fabric.

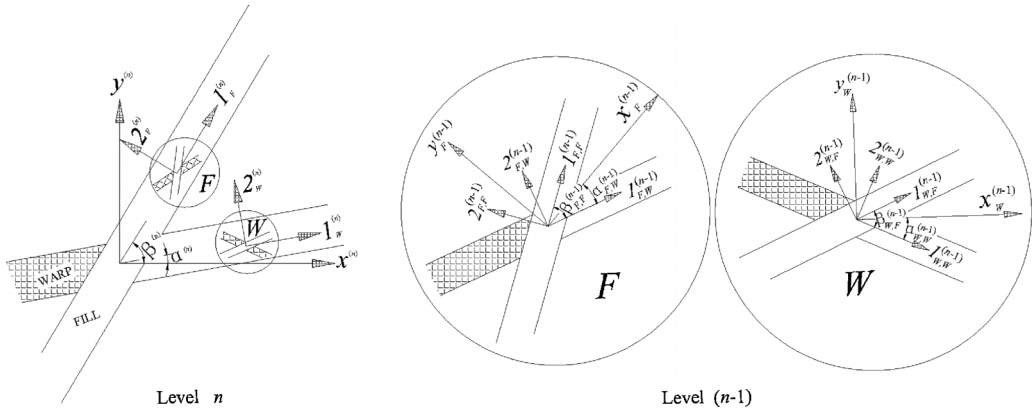

Fig. 7. Schematic of the hierarchical tissue.

L_{FH} are no longer equal to zero (for the previous case, in fact, $s+t=p+q=1$):

$$L_{WH}=(s+t-1)l_F; L_{FH}=(p+q-1)l_W \tag{21}$$

where, s and t (p and q) are the numbers of fill (warp) yarns above and below warp (fill) yarns in the representative unit cell, see Figure 6; l_F or l_W is yarn-to-yarn distance in the fill or warp direction.

General Hierarchical Theory

At each hierarchical level, the structure is modeled as a continuum medium.[38] For the sake of simplicity, we begin by neglecting the matrix (Fig. 7).

The level 1 structure has four independent geometric parameters, i.e., the two volumetric fractions and the two orientation angles, the level 2 structure has twelve independent geometric parameters, and a tissue composed by n hierarchical levels has $4\times(2^n-1)$ independent geometric parameters, in addition to the eight elastic constants of the two materials at level 0.

Level 1 structure:

We define the level 0 structure as a single yarn (fill or warp) which is composed by parallel fibers. Equations 3–6 can be rewritten as:

$$[Q]_F^{(0)}=\left[T\left(\beta^{(1)}\right)\right]^{-1}[Q^*]_F^{(0)}\left[T\left(\beta^{(1)}\right)\right] \tag{22}$$

$$[Q^*]_F^{(0)}=\begin{pmatrix} Q^{*(0)}_{11,F} & Q^{*(0)}_{12,F} & 0 \\ Q^{*(0)}_{21,F} & Q^{*(0)}_{22,F} & 0 \\ 0 & 0 & 2Q^{*(0)}_{66,F} \end{pmatrix} \tag{23}$$

with

$$Q^{*(0)}_{11,F}=\frac{E^{(0)}_{1,F}}{1\text{-}\upsilon^{(0)}_{12,F}\upsilon^{(0)}_{21,F}},\ Q^{*(0)}_{12,F}=\frac{\upsilon^{(0)}_{21,F}E^{(0)}_{1,F}}{1\text{-}\upsilon^{(0)}_{12,F}\upsilon^{(0)}_{21,F}},$$

$$Q^{*(0)}_{22,F}=\frac{E^{(0)}_{2,F}}{1\text{-}\upsilon^{(0)}_{12,F}\upsilon^{(0)}_{21,F}},\ Q^{*(0)}_{66,F}=G^{(0)}_{12,F}$$

$$[Q]_F^{(0)}=\begin{pmatrix} Q^{(0)}_{11,F} & Q^{(0)}_{12,F} & 2Q^{(0)}_{16,F} \\ Q^{(0)}_{21,F} & Q^{(0)}_{22,F} & 2Q^{(0)}_{26,F} \\ Q^{(0)}_{61,F} & Q^{(0)}_{62,F} & 2Q^{(0)}_{66,F} \end{pmatrix} \tag{24}$$

$$\left[T(\beta^{(1)})\right]=\begin{pmatrix} \cos^2\beta^{(1)} & \sin^2\beta^{(1)} & 2\cos\beta^{(1)}\sin\beta^{(1)} \\ \sin^2\beta^{(1)} & \cos^2\beta^{(1)} & -2\cos\beta^{(1)}\sin\beta^{(1)} \\ -\cos\beta^{(1)}\sin\beta^{(1)} & \cos\beta^{(1)}\sin\beta^{(1)} & \cos^2\beta^{(1)}-\sin^2\beta^{(1)} \end{pmatrix} \tag{25}$$

Substituting the subscript F with W and the orientation angle β with α, the properties of warp yarns can be deduced.

The elastic matrices of warp and fill yarns at the 0th level transformed from the local coordinate systems to the global coordinate system, can be expressed as:

$$\begin{cases} [Q]^{(0)}_{F,F}=\left[T\left(\beta^{(1)}_{F,F}\right)\right]^{-1}[Q^*]_F^{(0)}\left[T\left(\beta^{(1)}_{F,F}\right)\right] \\ [Q]^{(0)}_{F,W}=\left[T\left(\alpha^{(1)}_{F,W}\right)\right]^{-1}[Q^*]_W^{(0)}\left[T\left(\alpha^{(1)}_{F,W}\right)\right] \end{cases};\ \begin{cases} [Q]^{(0)}_{W,F}=\left[T\left(\beta^{(1)}_{W,F}\right)\right]^{-1}[Q^*]_F^{(0)}\left[T\left(\beta^{(1)}_{W,F}\right)\right] \\ [Q]^{(0)}_{W,W}=\left[T\left(\alpha^{(1)}_{W,W}\right)\right]^{-1}[Q^*]_W^{(0)}\left[T\left(\alpha^{(1)}_{W,W}\right)\right] \end{cases} \tag{26}$$

RESEARCH ARTICLE

By volumetric averaging, the final result for the 1st level is found:

$$\begin{cases} [Q]_F^{(1)} = v_{F,F}^{(1)}[Q]_{F,F}^{(0)} + v_{F,W}^{(1)}[Q]_{F,W}^{(0)} = v_{F,F}^{(1)}\left(\left[T\left(\beta_{F,F}^{(1)}\right)\right]^{-1}[Q^*]_F^{(0)}\left[T\left(\beta_{F,F}^{(1)}\right)\right]\right) + v_{F,W}^{(1)}\left(\left[T\left(\alpha_{F,W}^{(1)}\right)\right]^{-1}[Q^*]_W^{(0)}\left[T\left(\alpha_{F,W}^{(1)}\right)\right]\right) \\ [Q]_W^{(1)} = v_{W,F}^{(1)}[Q]_{W,F}^{(0)} + v_{W,W}^{(1)}[Q]_{W,W}^{(0)} = v_{W,F}^{(1)}\left(\left[T\left(\beta_{W,F}^{(1)}\right)\right]^{-1}[Q^*]_F^{(0)}\left[T\left(\beta_{W,F}^{(1)}\right)\right]\right) + v_{W,W}^{(1)}\left(\left[T\left(\alpha_{W,W}^{(1)}\right)\right]^{-1}[Q^*]_W^{(0)}\left[T\left(\alpha_{W,W}^{(1)}\right)\right]\right) \end{cases} \quad (27)$$

Employing Equations 19 and 20, the fiber volumes and volumetric fractions in warp and fill yarns can be determined:

$$V_{F,F}^{(1)} = N_{F,F}^{(1)}A_{F,F}^{(0)}L_{F,F}^{(1)}, V_{F,W}^{(1)} = N_{F,W}^{(1)}A_{F,W}^{(0)}L_{F,W}^{(1)}, V_{W,F}^{(1)} = N_{W,F}^{(1)}A_{W,F}^{(0)}L_{W,F}^{(1)}, V_{W,W}^{(1)} = N_{W,W}^{(1)}A_{W,W}^{(0)}L_{W,W}^{(1)} \quad (28)$$

$$v_{F,F}^{(1)} = \frac{V_{F,F}^{(1)}}{V_{F,U}^{(1)}}; v_{F,W}^{(1)} = \frac{V_{F,W}^{(1)}}{V_{F,U}^{(1)}}; v_{W,F}^{(1)} = \frac{V_{W,F}^{(1)}}{V_{W,U}^{(1)}}; v_{W,W}^{(1)} = \frac{V_{W,W}^{(1)}}{V_{W,U}^{(1)}} \quad (29)$$

$A_{F,F}^{(0)}$, $A_{F,W}^{(0)}$, $A_{W,F}^{(0)}$, and $A_{W,W}^{(0)}$ are calculated using Equation 12; $L_{F,F}^{(1)}$, $L_{F,W}^{(1)}$, $L_{W,F}^{(1)}$, and $L_{W,W}^{(1)}$ are obtained thanks to Equations 16, 17, and 21.

Level 2 structure:

Similarly, for the second level we can write:

$$\begin{cases} [Q]_{F,F}^{(1)} = \left[T\left(\beta_{F,F}^{(2)}\right)\right]^{-1}[Q^*]_F^{(1)}\left[T\left(\beta_{F,F}^{(2)}\right)\right] \\ [Q]_{F,W}^{(1)} = \left[T\left(\alpha_{F,W}^{(2)}\right)\right]^{-1}[Q^*]_W^{(1)}\left[T\left(\alpha_{F,W}^{(2)}\right)\right] \end{cases}; \begin{cases} [Q]_{W,F}^{(1)} = \left[T\left(\beta_{W,F}^{(2)}\right)\right]^{-1}[Q^*]_F^{(1)}\left[T\left(\beta_{W,F}^{(2)}\right)\right] \\ [Q]_{W,W}^{(1)} = \left[T\left(\alpha_{W,W}^{(2)}\right)\right]^{-1}[Q^*]_W^{(1)}\left[T\left(\alpha_{W,W}^{(2)}\right)\right] \end{cases} \quad (30)$$

$$\begin{cases} [Q]_F^{(2)} = v_{F,F}^{(2)}[Q]_{F,F}^{(1)} + v_{F,W}^{(2)}[Q]_{F,W}^{(1)} = v_{F,F}^{(2)}\left(\left[T\left(\beta_{F,F}^{(2)}\right)\right]^{-1}[Q^*]_F^{(1)}\left[T\left(\beta_{F,F}^{(2)}\right)\right]\right) + v_{F,W}^{(2)}\left(\left[T\left(\alpha_{F,W}^{(2)}\right)\right]^{-1}[Q^*]_W^{(1)}\left[T\left(\alpha_{F,W}^{(2)}\right)\right]\right) \\ [Q]_W^{(2)} = v_{W,F}^{(2)}[Q]_{W,F}^{(1)} + v_{W,W}^{(2)}[Q]_{W,W}^{(1)} = v_{W,F}^{(2)}\left(\left[T\left(\beta_{W,F}^{(2)}\right)\right]^{-1}[Q^*]_F^{(1)}\left[T\left(\beta_{W,F}^{(2)}\right)\right]\right) + v_{W,W}^{(2)}\left(\left[T\left(\alpha_{W,W}^{(2)}\right)\right]^{-1}[Q^*]_W^{(1)}\left[T\left(\alpha_{W,W}^{(2)}\right)\right]\right) \end{cases} \quad (31)$$

$$V_{F,F}^{(2)} = N_{F,F}^{(2)}A_{F,F}^{(1)}L_{F,F}^{(2)}, V_{F,W}^{(2)} = N_{F,W}^{(2)}A_{F,W}^{(1)}L_{F,W}^{(2)}, V_{W,F}^{(2)} = N_{W,F}^{(2)}A_{W,F}^{(1)}L_{W,F}^{(2)}, V_{W,W}^{(2)} = N_{W,W}^{(2)}A_{W,W}^{(1)}L_{W,W}^{(2)} \quad (32)$$

$$v_{F,F}^{(2)} = \frac{V_{F,F}^{(2)}}{V_{F,U}^{(2)}}; v_{F,W}^{(2)} = \frac{V_{F,W}^{(2)}}{V_{F,U}^{(2)}}; v_{W,F}^{(2)} = \frac{V_{W,F}^{(2)}}{V_{W,U}^{(2)}}; v_{W,W}^{(2)} = \frac{V_{W,W}^{(2)}}{V_{W,U}^{(2)}} \quad (33)$$

Level n structure:

Thus, in general, we have:

$$\begin{cases} [Q]_{F,F}^{(n-1)} = \left[T\left(\beta_{F,F}^{(n)}\right)\right]^{-1}[Q^*]_F^{(n-1)}\left[T\left(\beta_{F,F}^{(n)}\right)\right] \\ [Q]_{F,W}^{(n-1)} = \left[T\left(\alpha_{F,W}^{(n)}\right)\right]^{-1}[Q^*]_W^{(n-1)}\left[T\left(\alpha_{F,W}^{(n)}\right)\right] \end{cases}; \begin{cases} [Q]_{W,F}^{(n-1)} = \left[T\left(\beta_{W,F}^{(n)}\right)\right]^{-1}[Q^*]_F^{(n-1)}\left[T\left(\beta_{W,F}^{(n)}\right)\right] \\ [Q]_{W,W}^{(n-1)} = \left[T\left(\alpha_{W,W}^{(n)}\right)\right]^{-1}[Q^*]_W^{(n-1)}\left[T\left(\alpha_{W,W}^{(n)}\right)\right] \end{cases} \quad (34)$$

$$\begin{cases} [Q]_F^{(n)} = v_{F,F}^{(n)}[Q]_{F,F}^{(n-1)} + v_{F,W}^{(n)}[Q]_{F,W}^{(n-1)} = v_{F,F}^{(n)}\left(\left[T\left(\beta_{F,F}^{(n)}\right)\right]^{-1}[Q^*]_F^{(n-1)}\left[T\left(\beta_{F,F}^{(n)}\right)\right]\right) + v_{F,W}^{(n)}\left(\left[T\left(\alpha_{F,W}^{(n)}\right)\right]^{-1}[Q^*]_W^{(n-1)}\left[T\left(\alpha_{F,W}^{(n)}\right)\right]\right) \\ [Q]_W^{(n)} = v_{W,F}^{(n)}[Q]_{W,F}^{(n-1)} + v_{W,W}^{(n)}[Q]_{W,W}^{(n-1)} = v_{W,F}^{(n)}\left(\left[T\left(\beta_{W,F}^{(n)}\right)\right]^{-1}[Q^*]_F^{(n-1)}\left[T\left(\beta_{W,F}^{(n)}\right)\right]\right) + v_{W,W}^{(n)}\left(\left[T\left(\alpha_{W,W}^{(n)}\right)\right]^{-1}[Q^*]_W^{(n-1)}\left[T\left(\alpha_{W,W}^{(n)}\right)\right]\right) \end{cases} \quad (35)$$

$$V_{F,F}^{n} = N_{F,F}^{(n)}A_{F,F}^{(n-1)}L_{F,F}^{(n)}, V_{F,W}^{(n)} = N_{F,W}^{(n)}A_{F,W}^{(n-1)}L_{F,W}^{(n)}, V_{W,F}^{(n)} = N_{W,F}^{(n)}A_{W,F}^{(n-1)}L_{W,F}^{(n)}, V_{W,W}^{(n)} = N_{W,W}^{(n)}A_{W,W}^{(n-1)}L_{W,W}^{(n)} \quad (36)$$

$$v_{F,F}^{(n)} = \frac{V_{F,F}^{(n)}}{V_{F,U}^{(n)}}; v_{F,W}^{(n)} = \frac{V_{F,W}^{(n)}}{V_{F,U}^{(n)}}; v_{W,F}^{(n)} = \frac{V_{W,F}^{(n)}}{V_{W,U}^{(n)}}; v_{W,W}^{(n)} = \frac{V_{W,W}^{(n)}}{V_{W,U}^{(n)}} \quad (37)$$

This process can also be used in the presence of just one type of fiber, e.g., by removing the warp yarns. Then, simplifying Equations 34 and 35 and adding the matrix term, we have:

$$[Q]^{(n)} = \prod_{i=1}^{n} v_f^{(i)} \times \left[T\left(\sum_{i=1}^{n}\beta^{(i)}\right)\right]^{-1}[Q^*]_f^{(0)}\left[T\left(\sum_{i=1}^{n}\beta^{(i)}\right)\right] + \left(1 - \prod_{i=1}^{n} v_f^{(i)}\right)[Q]_M \quad (38)$$

where $v_f^{(i)}$ and $\beta^{(i)}$ are the volumetric fraction and orientation angle of the fiber at the ith level, respectively; $[Q^*]_f^{(0)}$, $[Q]_M$ is the stiffness matrix of the fiber at the 0th level in the local coordinate system and the matrix.

Self-Similar Hierarchical Structures

The general hierarchical theory is complicated and in order to explain the process in a simple way, two kinds of self-similar hierarchical structures (Fig. 8(a) and (b)) are introduced here.

Self-Similar Case (1)

In this case, the global coordinate systems of fill and warp yarns at the $(n-1)$th level are coincident with the local coordinate systems of fill and warp yarns at the nth level, respectively; the configuration satisfies a set of self-similar conditions:

$$v_{F,F}^{(i)} = v_{W,F}^{(i)} = v_F;\ v_{F,W}^{(i)} = v_{W,W}^{(i)} = v_W,\ \beta_{F,F}^{(i)} = \beta_{W,F}^{(i)} = \beta,\ \alpha_{F,W}^{(i)} = \alpha_{W,W}^{(i)} = \alpha \tag{39}$$

Thus, fill and warp yarns have identical sub-structure, i.e., $[Q^*]_F^{(i)} = [Q^*]_W^{(i)}$.

Level 1 structure:

Basing on Figure 8(a) and the self-similar condition (Eq. 39), Equation 27 becomes:

$$[Q]_F^{(1)} = [Q]_W^{(1)} = v_F\left([T(\beta)]^{-1}[Q^*]_F^{(0)}[T(\beta)]\right) + v_W\left([T(\alpha)]^{-1}[Q^*]_W^{(0)}[T(\alpha)]\right) \tag{40}$$

Level 2 structure:

Correspondingly, the elastic matrices at the second level are expressed as:

$$[Q]_F^{(2)} = [Q]_W^{(2)} = v_F^2\left([T(2\beta)]^{-1}[Q^*]_F^{(0)}[T(2\beta)]\right) + v_F v_W\left([T(\alpha+\beta)]^{-1}\left[[Q^*]_F^{(0)} + [Q^*]_W^{(0)}\right][T(\alpha+\beta)]\right) + v_W^2\left([T(2\alpha)]^{-1}[Q^*]_W^{(0)}[T(2\alpha)]\right) \tag{41}$$

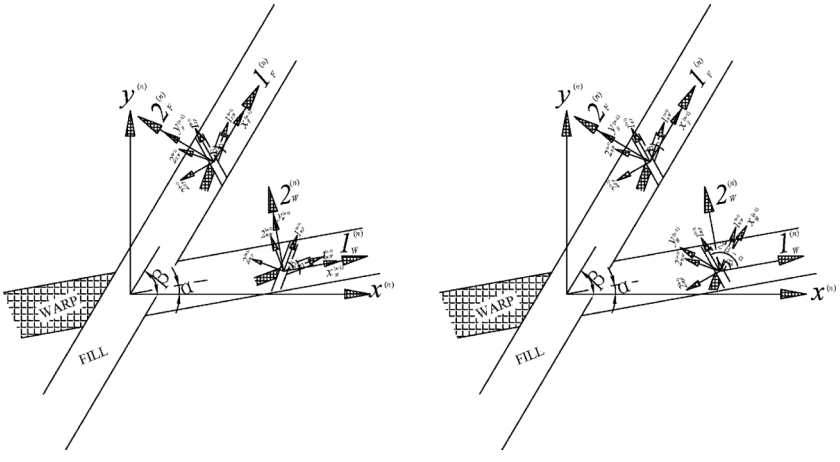

Fig. 8. Schematic of the self-similar hierarchical structures.

Level n structure:

Likewise, using the recursive process and compacting the result, we find the elastic matrix of the nth level as:

$$[Q]_F^{(n)} = [Q]_W^{(n)} = \sum_{i=0}^{n} v_F^{n-i} v_W^i \Big([T(i\alpha + (n-i)\beta)]^{-1} \times \left[a_{n,i}[Q^*]_F^{(0)} + b_{n,i}[Q^*]_W^{(0)}\right][T(i\alpha + (n-i)\beta)]\Big) \tag{42}$$

where the coefficients ($a_{n,i}$, $b_{n,i}$) satisfy the following recursive relationship:

$$\begin{cases} a_{n,i} = a_{n-1,i-1} + a_{n-1,i} \\ b_{n,i} = b_{n-1,i-1} + b_{n-1,i} \\ C_n^i = a_{n,i} + b_{n,i} \end{cases} \tag{43}$$

with combination C_n^i.

Let us define $v_f = v_F + v_W$ as the fiber volumetric fraction and $\theta_i = n\beta + i(\alpha-\beta)$, $\lambda = V_W/V_F$. Considering the filling of a matrix, we have:

$$\begin{aligned}[Q]^{(n)} &= \sum_{i=0}^{n} v_F^{n-i} v_W^i \Big([T(n\beta + i(\alpha-\beta)]^{-1}\left[a_{n,i}[Q^*]_F^{(0)} + b_{n,i}[Q^*]_W^{(0)}\right] \times [T(n\beta + i(\alpha-\beta)]\Big) + \left(1 - v_f^n\right)[Q]_M \\ &= \sum_{i=0}^{n} a_{n,i} v_f^n \frac{\lambda^i}{(1+\lambda)^n}\left([T(\theta_i)]^{-1}[Q^*]_F^{(0)}[T(\theta_i)]\right) + \sum_{i=0}^{n} b_{n,i} v_f^n \frac{\lambda^i}{(1+\lambda)^n}\left([T(\theta_i)]^{-1}[Q^*]_W^{(0)}[T(\theta_i)]\right) + \left(1 - v_f^n\right)[Q]_M \end{aligned} \tag{44}$$

The coefficients ($a_{n,i}$, $b_{n,i}$) are listed in Table 1 for $n = 1$–8.

Furthermore, if volumetric fractions of fill and warp yarns are equal, i.e., $v_F = v_W$, Equation 44 becomes:

$$[Q]^{(n)} = \left(\frac{v_f}{2}\right)^n \sum_{i=0}^{n} a_{n,i}\left([T(\theta_i)]^{-1}[Q^*]_F^{(0)}[T(\theta_i)]\right) + \left(\frac{v_f}{2}\right)^n \sum_{i=0}^{n} b_{n,i}\left([T(\theta_i)]^{-1}[Q^*]_W^{(0)}[T(\theta_i)]\right) + \left(1 - v_f^n\right)[Q]_M \tag{45}$$

Finally, when $[Q^*]_F^{(0)} = [Q^*]_W^{(0)} = [Q^*]_f^{(0)}$ and $\beta = \alpha$, from Equation 45, we have:

$$[Q]^{(n)} = v_f^n\left([T(n\beta)]^{-1}[Q^*]_f^{(0)}[T(n\beta)]\right) + \left(1 - v_f^n\right)[Q]_M \tag{46}$$

Equation 46, which can also be obtained from Equation 38 using the self-similar conditions (Eq. 39), suggests that our theory is self-consistent.

Self-Similar Case (2)

In this case, the global coordinate systems of the $(n-1)$th level in fill and warp yarns are

RESEARCH ARTICLE

Table 1. Coefficients ($a_{n,i}$, $b_{n,i}$) for n = 1–8.

n	($a_{n,0}$, $b_{n,0}$)	($a_{n,1}$, $b_{n,1}$)	($a_{n,2}$, $b_{n,2}$)	($a_{n,3}$, $b_{n,3}$)	($a_{n,4}$, $b_{n,4}$)	(a_{n5}, $b_{n,5}$)	($a_{n,6}$, $b_{n,6}$)	($a_{n,7}$, $b_{n,7}$)	($a_{n,8}$, $b_{n,8}$)
1	(1,0)	(0,1)	–	–	–	–	–	–	–
2	(1,0)	(1,1)	(0,1)	–	–	–	–	–	–
3	(1,0)	(2,1)	(1,2)	(0,1)	–	–	–	–	–
4	(1,0)	(3,1)	(3,3)	(1,3)	(0,1)	–	–	–	–
5	(1,0)	(4,1)	(6,4)	(4,6)	(1,4)	(0,1)	–	–	–
6	(1,0)	(5,1)	(10,5)	(10,10)	(5,10)	(1,5)	(0,1)	–	–
7	(1,0)	(6,1)	(15,6)	(20,15)	(15,20)	(6,15)	(1,6)	(0,1)	–
8	(1,0)	(7,1)	(21,7)	(35,21)	(35,35)	(21,35)	(7,21)	(1,7)	(0,1)

both coincident with the local coordinate system of fill yarns at the nth level; and the configuration satisfies another set of self-similar conditions:

$$v_{F,F}^{(i)} = v_{W,F}^{(i)} = v_F,\ v_{F,W}^{(i)} = v_{W,W}^{(i)} = v_W;\ \beta_{F,F}^{(i)} = \beta,\ \beta_{W,F}^{(i)} = 2\beta - \alpha,\ \alpha_{F,W}^{(i)} = \alpha,\ \alpha_{W,W}^{(i)} = \beta \tag{47}$$

Thus, warp and fill yarns are composed of parallel sub-fibers i.e., $[Q]_F^{(i)} = [Q]_W^{(i)}$.

Based on Figure 8(b) and the self-similar conditions (Eq. 47), like case (1), the results from the 1st level to nth level are expressed as:

Level 1 structure:

$$[Q]_F^{(1)} = [Q]_W^{(1)} = v_F\left([T(\beta)]^{-1}[Q^*]_F^{(0)}[T(\beta)]\right) + v_W\left([T(\alpha)]^{-1}[Q^*]_W^{(0)}[T(\alpha)]\right) \tag{48}$$

Level 2 structure:

$$[Q]_F^{(2)} = [Q]_W^{(2)} = (v_F + v_W)\left(v_F\left([T(\beta)]^{-1}[Q^*]_F^{(0)}[T(\beta)]\right) + v_W\left([T(\alpha)]^{-1}[Q^*]_W^{(0)}[T(\alpha)]\right)\right) \tag{49}$$

Level n structure:

$$[Q]_F^{(n)} = [Q]_W^{(n)} = (v_F + v_W)^{n-1}\left(v_F\left([T(n\beta)]^{-1}[Q^*]_F^{(0)}[T(n\beta)]\right) + v_W\left([T(\alpha + (n-1)\beta)]^{-1}[Q^*]_W^{(0)}[T(\alpha + (n-1)\beta)]\right)\right) \tag{50}$$

Defining $v_f = v_F + v_W$ and $\lambda = V_W/V_F$ and considering the effect of the matrix, Equation 50 becomes:

If volumetric fractions of fill and warp yarns are equal, i.e., $v_F = v_W$, Equation 51 can be written as:

$$[Q]^{(n)} = \frac{v_f^n}{2}\left([T(n\beta)]^{-1}[Q^*]_F^{(0)}[T(n\beta)]\right) + \frac{v_f^n}{2}\left([T(n\beta + \alpha - \beta)]^{-1}[Q^*]_W^{(0)}[T(n\beta + \alpha - \beta)]\right) + \left(1 - v_f^n\right)[Q]_M \tag{52}$$

If $[Q^*]_F^{(0)} = [Q^*]_W^{(0)} = [Q^*]_f^{(0)}$ and $\beta = \alpha$, Equation 52 is further simplified:

$$[Q]^{(n)} = v_f^n[T(n\beta)]^{-1}[Q^*]_f^{(0)}[T(n\beta)] + (1 - v_f^n)[Q]_M \tag{53}$$

We can see that Equations 46 and 53 are identical, suggesting again the self-consistency of our approach.

Orthogonal Yarns for Both Self-Similar Hierarchical Structures

Case (1): If $\alpha = 0$ and $\beta = \frac{\pi}{2}$, Equation 44 becomes:

$$[Q]^{(n)} = \sum_{i=0}^{n} a_{n,i}v_F^{n-i}v_W^i\left(\left[T((n-i)\frac{\pi}{2})\right]^{-1}[Q^*]_F^{(0)}\left[T((n-i)\frac{\pi}{2})\right]\right) + \sum_{i=0}^{n} b_{n,i}v_F^{n-i}v_W^i\left(\left[T((n-i)\frac{\pi}{2})\right]^{-1}[Q^*]_W^{(0)}\left[T((n-i)\frac{\pi}{2})\right]\right) + \left(1 - v_f^n\right)[Q]_M \tag{54}$$

It can be seen that the transformation matrix is dependent on $(n - i)$; thus, the final expression is:

$$[Q]^{(n)} = v_f^{n-1}v_F\left([T(n\beta)]^{-1}[Q^*]_F^{(0)}[T(n\beta)]\right) + v_f^{n-1}v_W\left([T(n\beta + \alpha - \beta)]^{-1}[Q^*]_W^{(0)}[T(n\beta + \alpha - \beta)]\right) + \left(1 - v_f^n\right)[Q]_M = v_f^n\frac{1}{1+\lambda}\left([T(n\beta)]^{-1}[Q^*]_F^{(0)}[T(n\beta)]\right) + v_f^n\frac{\lambda}{1+\lambda}\left([T(n\beta + \alpha - \beta)]^{-1}[Q^*]_W^{(0)}[T(n\beta + \alpha - \beta)]\right) + \left(1 - v_f^n\right)[Q]_M \tag{51}$$

$$[Q]^{(n)} = \sum_{i=0}^{n} a_{n,i}v_F^{n-i}v_W^i\left(\frac{1-(-1)^{n-i}}{2}\left[\overrightarrow{Q^*}\right]_F^{(0)} + \frac{1+(-1)^{n-i}}{2}[Q^*]_F^{(0)}\right) + \sum_{i=0}^{n} b_{n,i}v_F^{n-i}v_W^i\left(\frac{1-(-1)^{n-i}}{2}\left[\overrightarrow{Q^*}\right]_W^{(0)} + \frac{1+(-1)^{n-i}}{2}[Q^*]_W^{(0)}\right) + \left(1 - v_f^n\right)[Q]_M \tag{55}$$

Table 2. Material constants of each level in tendon (MPa). "Theo" stands for theoretical predictions; "Ref" stands for reference values; "Input" stands for input parameters.

(0°)	Matrix	Molecule		Fibril		Fiber		Fascicle		Tendon
	Input	Theo	Ref	Theo	Ref	Theo	Ref	Theo	Ref	Input
E_1	1[42]	3536	350–12 000[21]	2397	2000–7000[26]	1534	150–1000[25]	1066	480–1390[44]	750[45]
E_2	1[42]	53.2	–	36.4	–	25.1	–	17.3	–	12[48]
μ_{12}	0.25	3.16	–	3.13	–	3.10	–	3.05	2.73[27]	2.98[49]
G_{12}	0.4	22.3	–	15.7	31–81[21]	10.7	27–50[43]	7.3	–	5[45]

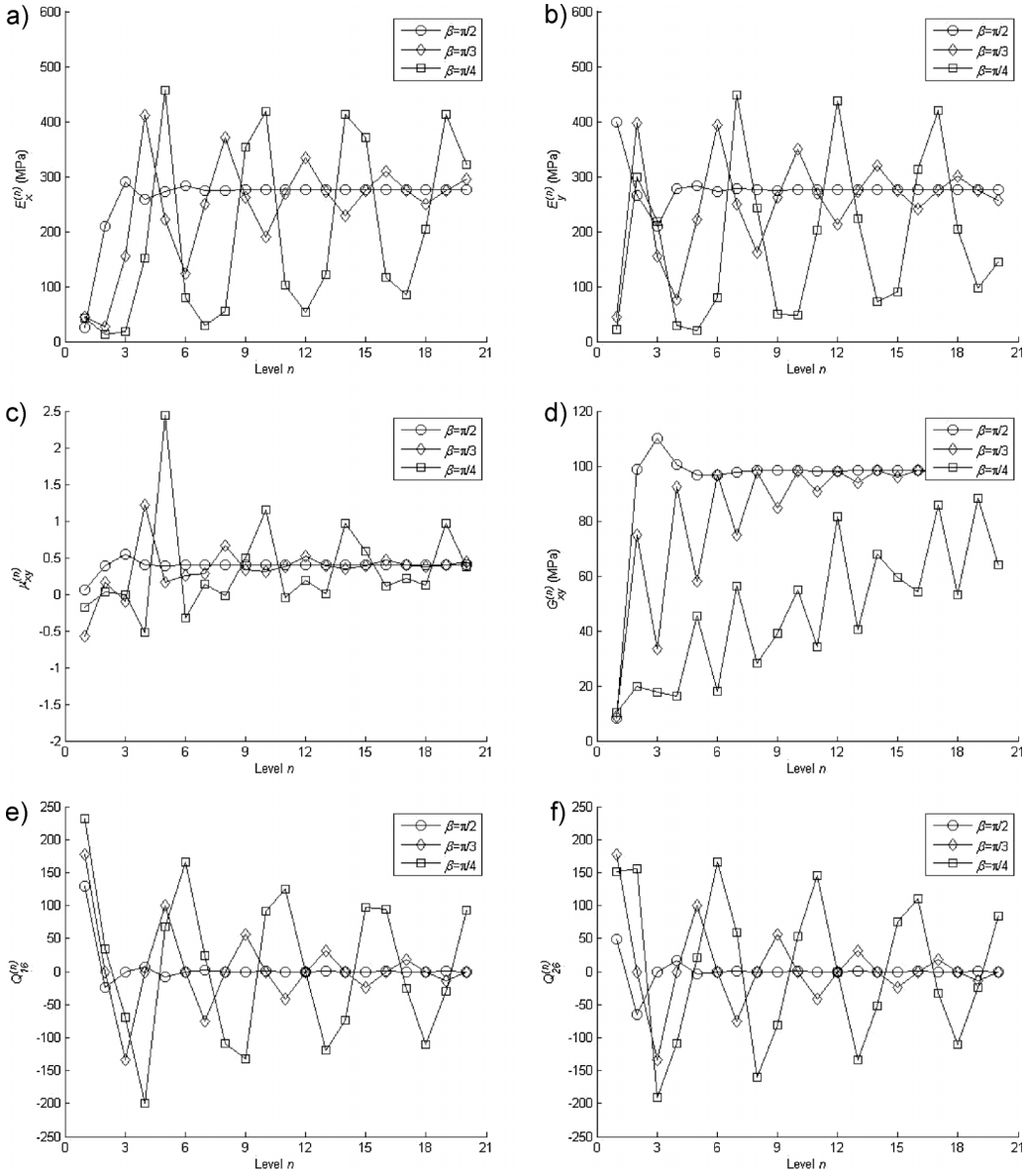

Fig. 9. Independent material constants and shear-coupling parameters with different orientation angles, for case (1).

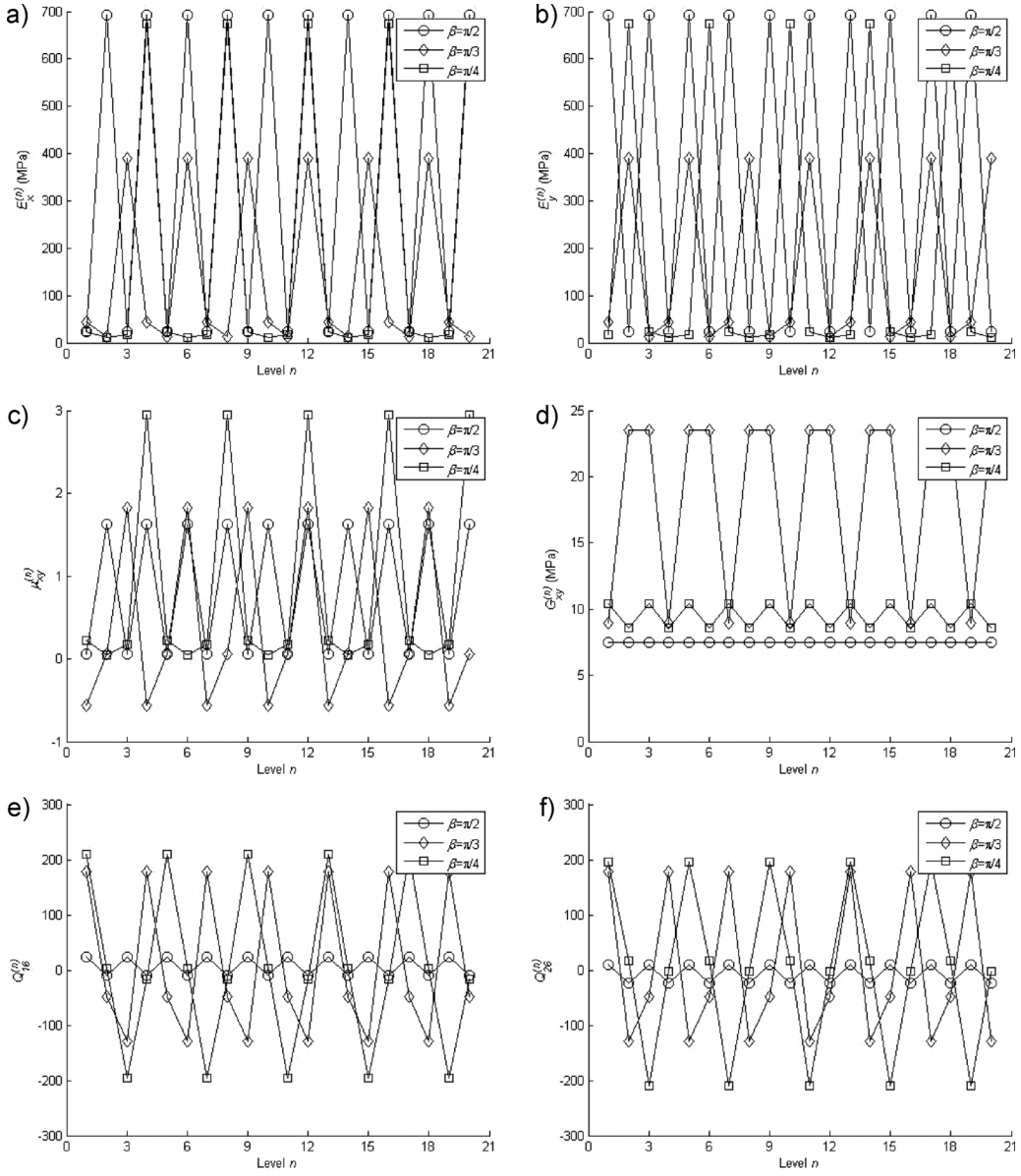

Fig. 10. Independent material constants and shear-coupling parameters with different orientation angles, for case (2).

Herein, matrices $[\overrightarrow{Q^*}]_F^{(0)}$ and $[\overrightarrow{Q^*}]_W^{(0)}$ can be obtained by transforming $[\overrightarrow{Q^*}]_F^{(0)}$ and $[\overrightarrow{Q^*}]_W^{(0)}$ with the transformation matrix $[T(90^\circ)]$.

Case (2): When $\alpha = 0$ and $\beta = (\pi/2)$, Equation 51 becomes:

$$[Q]^{(n)} = v_f^{n-1} v_F \left(\left[T\left(n\frac{\pi}{2}\right) \right]^{-1} [Q^*]_F^{(0)} \left[T\left(n\frac{\pi}{2}\right) \right] \right) + v_f^{n-1} v_W \left(\left[T\left((n-1)\frac{\pi}{2}\right) \right]^{-1} [Q^*]_W^{(0)} \left[T\left((n-1)\frac{\pi}{2}\right) \right] \right) + \left(1 - v_f^n\right)[Q]_M \tag{56}$$

The transformation matrix is dependent on n, and the final expression is:

$$[Q]^n = v_f^{n-1} v_F \left(\frac{1+(-1)^n}{2} [Q^*]_F^{(0)} + \frac{1-(-1)^n}{2} \left[\overrightarrow{Q^*}\right]_F^{(0)} \right) + v_f^{n-1} v_W \left(\frac{1+(-1)^n}{2} \left[\overrightarrow{Q^*}\right]_W^{(0)} + \frac{1-(-1)^n}{2} [Q^*]_W^{(0)} \right) + \left(1 - v_f^n\right)[Q]_M \tag{57}$$

where matrices $\left[\overrightarrow{Q^*}\right]_F^{(0)}$ and $\left[\overrightarrow{Q^*}\right]_W^{(0)}$ are the same as those introduced in Equation 55.

Parametric Analysis

Equations 44 and 51 hint that the elastic matrices at the nth level are dependent on the fiber orientation angles α and β and the relative volumetric ratio λ of warp to fill yarns when the total fiber volumetric fraction v_f^n is fixed. Here, assuming the two self-similar models, we investigate the influence of its specific components employing elastic parameters of a collagen molecule (Table 2). The changes of the six elastic parameters ($E_x^{(n)}$, $E_y^{(n)}$, $\mu_{xy}^{(n)}$, $G_{xy}^{(n)}$, $Q_{16}^{(n)}$, and $Q_{26}^{(n)}$, i.e., Young's moduli, Poisson's ratio, shear modulus, and shear-coupling parameters in global coordinate system of the hierarchical level n) are reported below.

Influence of Orientation Angles

In order to investigate the influence of the orientation angles, we fix $\alpha = 30^\circ$, $\lambda = 1.0$, and $v_f^n = 0.20$ and vary β. Three values of β are selected: $\pi/2$, $\pi/3$, and $\pi/4$. The comparisons of the six parameters defined above, for case (1) and case (2), are reported in Figure 9 and 10, respectively.

From Figure 9 we can see that the amplitude (denoted by A) of each parameter becomes greater as the orientation angle made by warp and fill yarns decreases; moreover, the rapidity of convergence also becomes slower. The reason is that the characteristic period is extended as the orientation angle decreases, reducing the rapidity of the homogenization. For Young's moduli $E_x^{(n)}$ and $E_y^{(n)}$, we note that they approach the same value, and are complementary at the same level (Fig. 9(a) and (b)). Poisson's ratio $\mu_{xy}^{(n)}$ tends to be 0.5 (Fig. 9(c)); however, when level n and the orientation angle are small, it is beyond the isotropic upper limit of 0.5 and even negative but within the isotropic lower limit of –1. This is due to the large difference between transverse and longitudinal Young's moduli of the collagen molecule. Shear

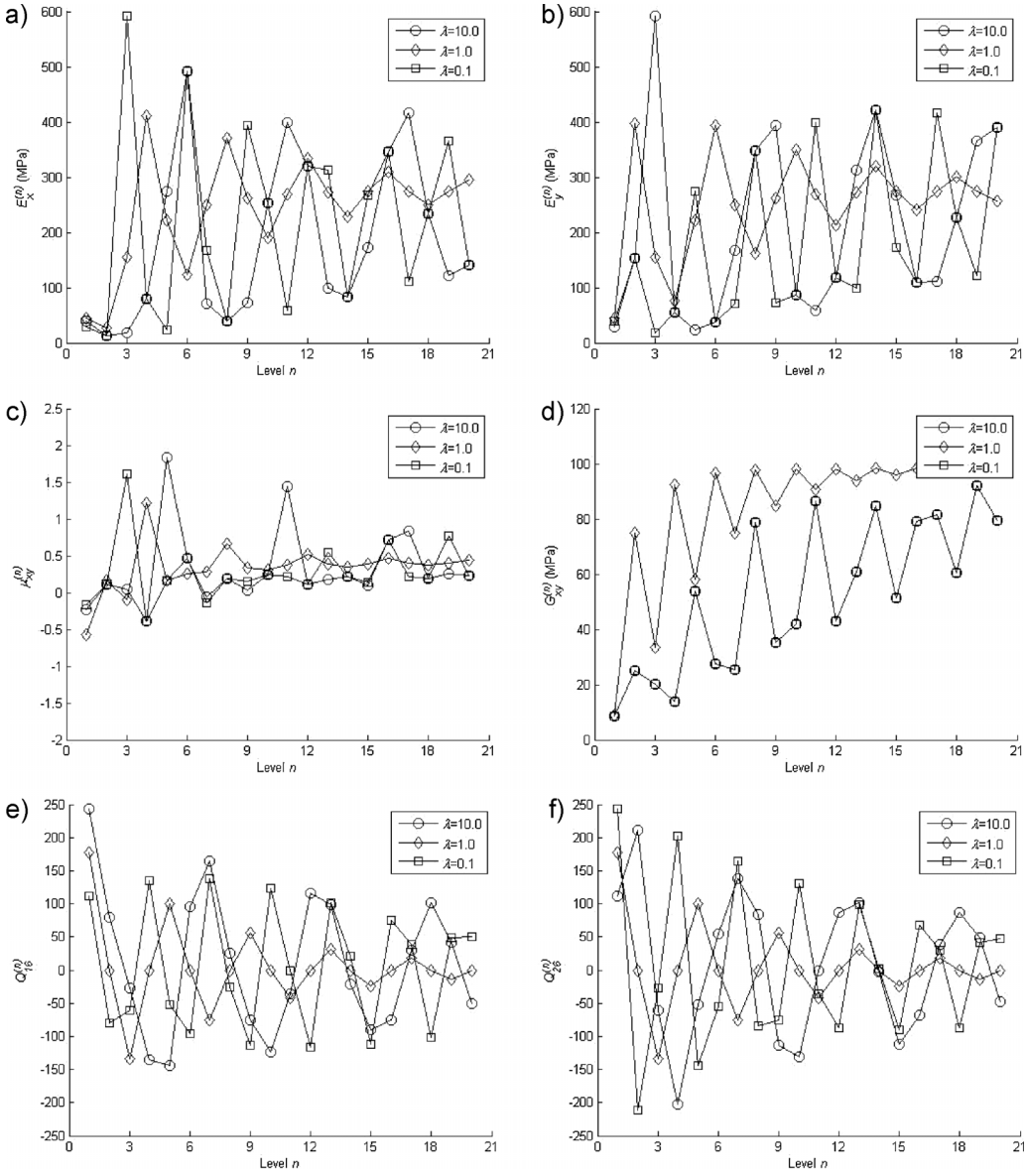

Fig. 11. Independent material constants and shear-coupling parameters with different relative volumetric ratios of warp yarns to fill yarns, for case (1).

RESEARCH ARTICLE

modulus $G_{xy}^{(n)}$ has a different behavior with respect to the other parameters. For different orientation angles, when n tends to infinity, an order relationship $G_{xy}^{(n)}(\pi/2) > G_{xy}^{(n)}(\pi/3) > G_{xy}^{(n)}(\pi/4)$ holds. Finally, $Q_{16}^{(n)}$ and $Q_{26}^{(n)}$ show that the shear-coupling effect for higher hierarchical level disappears, see Figure 9(e) and (f).

Figure 10 shows that the six elastic parameters share a characteristic of case (2), namely, the periodicity. Like in case (1), Young's moduli $E_x^{(n)}$, and $E_y^{(n)}$ (Fig. 10(a) and (b)) are complementary, but they do not approach a fixed value as n tends to infinity, and neither the amplitude (A) for each parameter shrinks (or extends) as the orientation angle made by warp and fill yarns decreases (e.g., for $E_x^{(n)}$,we find the relationship $A(\pi/2) \approx A(\pi/4) > A(\pi/3)$).

Influence of the Relative Volumetric Ratio of Warp to Fill Yarns

In order to investigate the influence of the relative volumetric ratio (λ) of warp to fill yarns, we fix $\alpha = 30^\circ$, $\beta = 60^\circ$, $v_f^n = 0.20$, and vary λ. Three values of λ are selected: 10.0, 1.0, and 0.1. The comparisons of the previous six parameters, for case (1) and case (2), are depicted in Figure 11 and 12, respectively.

In this situation, as n increases, the six parameters tend to constants more slowly for $\lambda = 10.0$ and $\lambda = 0.1$ than for $\lambda = 1.0$, and the amplitude (A) for $\lambda = 1.0$ shrinks regularly, while irregularly for $\lambda = 10.0$ and $\lambda = 0.1$ (see Fig. 11(b) and (d)). Young's moduli $E_x^{(n)}$ and $E_y^{(n)}$ and Poisson's ratio $\mu_{xy}^{(n)}$ converge to the same values of those for case (1) with varying

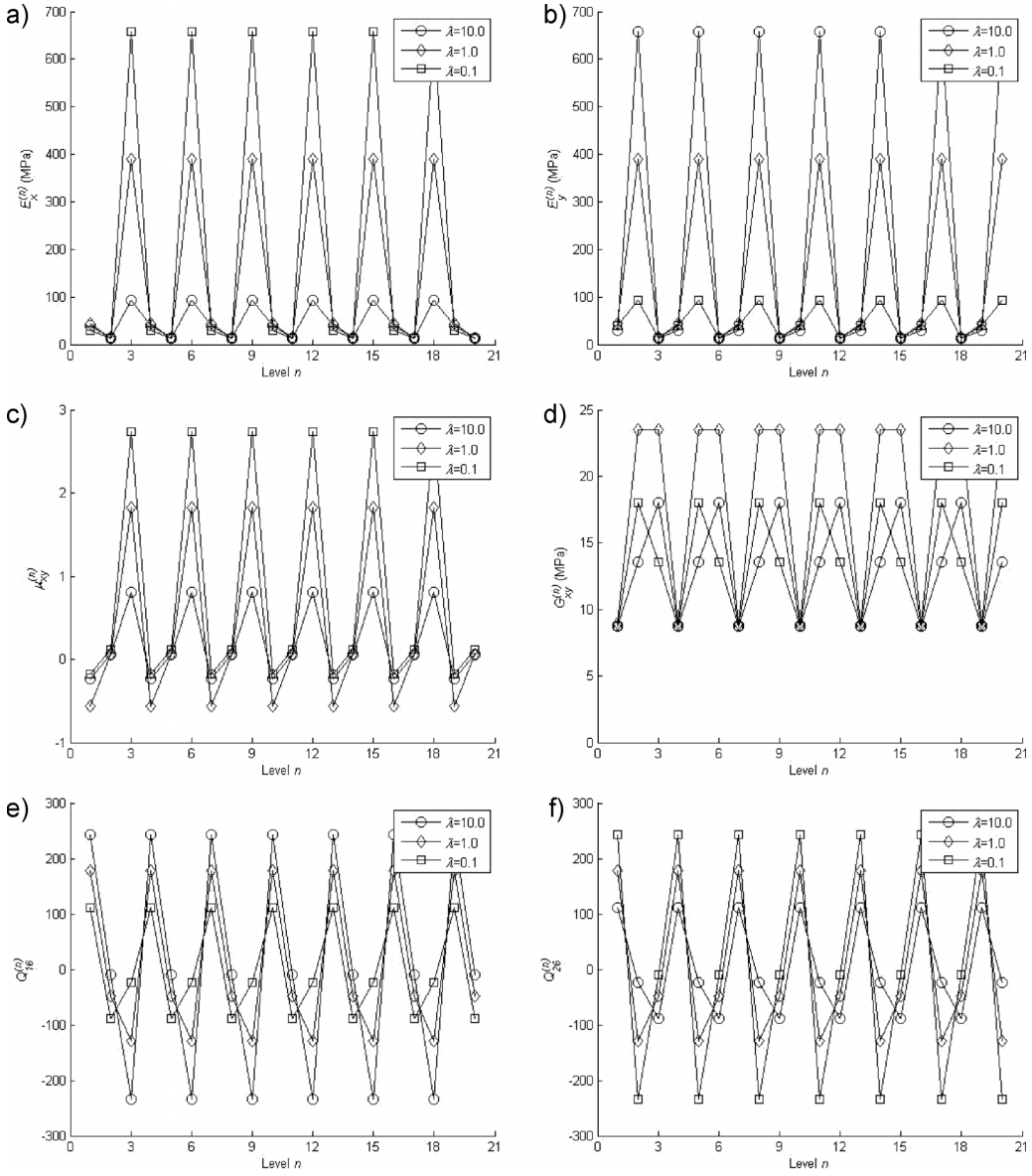

Fig. 12. Independent material constants and shear-coupling parameters with different relative volumetric ratios of warp yarns to fill yarns, for case (2).

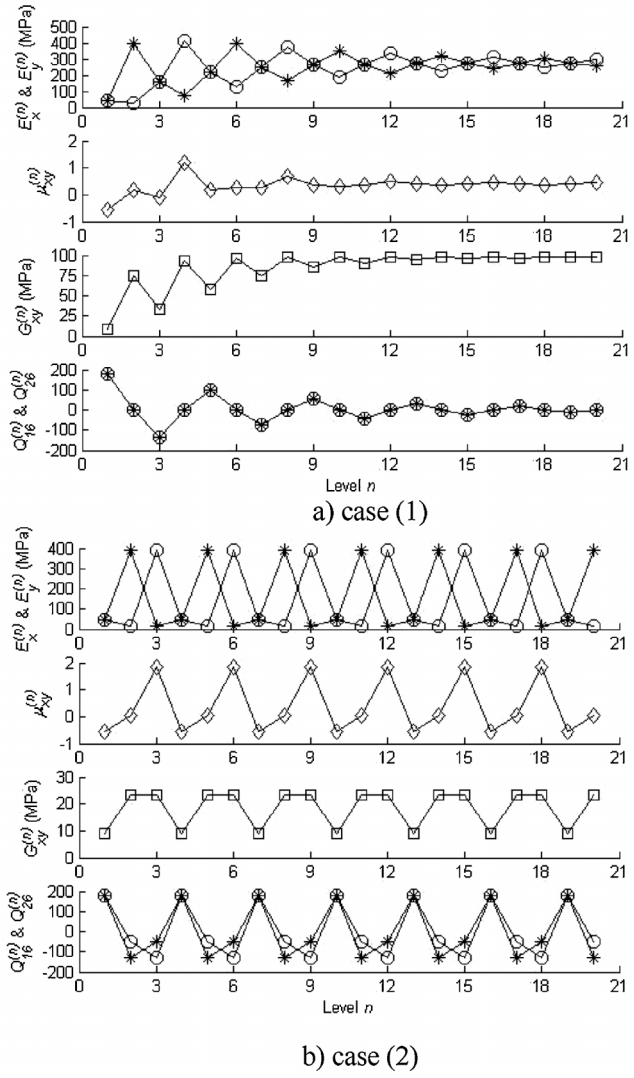

Fig. 13. Elements in the elastic matrices for both the two self-similar cases.

orientation angle, due to the same constituents. Regarding the shear modulus, we find $G_{xy}^{(n)}(1.0) > G_{xy}^{(n)}(10.0) \equiv G_{xy}^{(n)}(0.1)$. This is expected since $\lambda = 10.0$ and $\lambda = 0.1$ are equivalent to exchanging warp with fill yarns. Finally, the shear-coupling effect disappears as n tends to infinity.

For case (2), Figure 12 shows that Young's moduli $E_x^{(n)}$ and $E_y^{(n)}$ and shear-coupling parameters $Q_{16}^{(n)}$ and $Q_{26}^{(n)}$ are complementary at the same level (Fig. 12(a), (b), (e), and (f)) and the amplitudes (A) for these two pairs shrink or extend as the volumetric ratio of warp to fill yarns decreases, i.e., we find $A(0.1) > A(1.0) > A(10.0)$ for $E_x^{(n)}$ and $A(10.0) > A(1.0) > A(0.1))$ for $Q_{16}^{(n)}$. This also happens for the Poisson's ratio $\mu_{xy}^{(n)}$. As for the shear modulus, when $n = 3m+1$ ($m = 0, 1, 2...$), $G_{xy}^{(3m+1)}(10.0) = G_{xy}^{(3m+1)}(1.0) = G_{xy}^{(3m+1)}(0.1)$; when $n = 3m+2$ and $n = 3m+3$ ($m = 0, 1, 2...$), $G_{xy}^{(3m+2)}(0.1) = G_{xy}^{(3m+3)}(10.0) < G_{xy}^{(3m+2)}(1.0)$ and $G_{xy}^{(3m+2)}(10.0) = G_{xy}^{(3m+3)}(0.1) < G_{xy}^{(3m+2)}(1.0)$.

Comparison between Self-Similar Cases (1) and (2)

In order to select an appropriate structure to mimic a tissue, we compare the six elastic parameters of case (1) with those of case (2) by fixing the orientation angles $\alpha = 30^\circ$, $\beta = 60^\circ$, the volumetric ratio $\lambda = 1$ of warp to fill yarns and the total volumetric fraction of fiber $v_f^n = 0.20$. The results are reported in Figure 13.

Comparing Figure 9–12 with Figure 13 suggests the existence of a general regularity. In case (1), each elastic independent constant tends asymptotically to a fixed value. When the level number n is odd, $E_x^{(n)}$ and $E_y^{(n)}$ are equal; instead, when n is even, the gap between the two becomes smaller. In case (2), each constant has the same period π/β (in this case, the period is 3). When $n = 3m+1$ ($m = 0, 1, 2...$), $E_x^{(3m+1)} = E_y^{(3m+1)}$, while, when $n = 3m+2$ and $n = 3m+3$ ($m = 0, 1, 2...$), $E_x^{(3m+2)} = E_y^{(3m+3)}$ and $E_x^{(3m+3)} = E_y^{(3m+2)}$. Similarly, $\mu_{xy}^{(n)}$ and $G_{xy}^{(n)}$ oscillate periodically.

In fact, in case (1), as n approaches infinity, the whole structure becomes closer to a homogenous material. In case (2), this is due to the same arrangement of warp and fill yarns at each level; thus, the structure at different levels has an orientation periodicity.

Influence of the Constituents on the Overall Elasticity of Tendons

Volumetric Fractions of Collagen and Matrix

Tendons are constituted mainly of fibers of fibrous type I collagen and are dense, often parallel-fibered, tissues. Generally, tendon consists of about 20% cellular material and about 80% extracellular material; the extracellular material is further subdivided into about 30% solids and 70% water. These extracellular solids are collagen, proteoglycan, and a small amount of elastin.[2]

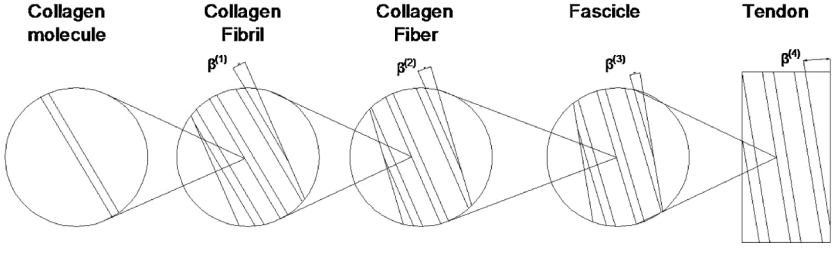

Fig. 14. Schematic of the hierarchical model of a tendon.

Here, tendon is treated as a woven hierarchical material only composed by fill yarns and as a composite material made by two phases, i.e., collagen and matrix. Proteoglycan and water are treated as the matrix. Mow *et al.*[39] give the weight percentages of the constituents in tendons, i.e., 23% for collagen, 7% for proteoglycan, and 70% for water. Thus, the volumetric fractions can be derived from the densities: 1.2 g·cm^{-2} for

Table 3. Material constants of each level with varying elastic constants of tendon (MPa). ''Theo'' stands for theoretical prediction.

(0°)	Matrix	Molecule		Fibril		Fiber		Fascicle		Tendon
	Input	Theo	Ref	Theo	Ref	Theo	Ref	Theo	Ref	Input
				Varying the longitudinal Young's modulus of tendon						
E_1	1[42]	680–5060	350–12 000[21]	463–3429	2000–7000[26]	317–2324	150–1000[25]	217–1577	480–1390[44]	150[46]–1070[47]
E_2	1[42]	53.2–53.4	–	36.4–36.5	–	24.9–25.0	–	17.2–17.3	–	12[48]
μ_{12}	0.25	3.04–3.16	–	3.03–3.14	–	3.02–3.10	–	3.00–3.05	2.73[27]	2.98[49]
G_{12}	0.4	22.3	–	15.2	31–81[21]	10.4	27–50[43]	7.2	–	5[45]
				Varying the longitudinal Poisson's ratio of tendon						
E_1	1[42]	3450–3568	350–12 000[21]	2346–2416	2000–7000[26]	1599–1636	150–1000[25]	1093–1108	480–1390[44]	750[45]
E_2	1[42]	53.1–53.3	–	36.3–36.4	–	24.9–25.0	–	17.2–17.2	–	12[48]
μ_{12}	0.25	0.43–5.77	–	0.43–5.74	–	0.43–5.70	–	0.43–5.65	2.73[27]	0.42–5.57[49]
G_{12}	0.4	22.3	–	15.2	31–81[21]	10.4	27–50[43]	7.2	–	5[45]
				Varying the longitudinal shear modulus of tendon						
E_1	1[42]	3536	350–12 000[21]	2397	2000–7000[26]	1626	150–1000[25]	1104	480–1390[44]	750[45]
E_2	1[42]	53.2	–	36.4	–	25.0	–	17.2	–	12[48]
μ_{12}	0.25	3.16	–	3.13	–	3.10	–	3.05	2.73[27]	2.98[49]
G_{12}	0.4	93.7–950.9	–	63.6–643.9	31–81[21]	43.2–436.0	27–50[43]	29.4–295.3	–	20–200[22][23][50]

collagen,[40] 1.4 g cm^{-2} for proteoglycan,[41] and 1.0 g cm^{-2} for water. Accordingly, the volumetric fractions 79% and 21% are calculated for matrix and collagen, respectively.

Influence of Different Variables

The considered architecture is show in Figure 14. As discussed before, tendons are defined as a parallel-fibered tissue, i.e., the included angles made by $(i-1)$th and ith levels is equal to zero. Under the conditions of $v_f^{(i)} = 0.667$, easily deduced from $v_f = 21\%$, and $\beta^{(i)} = 0$, the elastic constants of the collagen molecules are derived from the experimental data of the tendon and matrix. Moreover, the material constants of collagen fibril, collagen fiber, and fascicle are also derived by employing Equation 38. These results are reported in Table 2.

By investigating the upper and lower bound of the elastic constants of each level of tendons, the influences of different variables are reported in Table 3. The results show that these influences are mainly controlled by the reciprocal theorem, namely $E_1\mu_{21} = E_2\mu_{12}$. However, the shear modulus produces no influence on the other constants; the reason is that the orthotropic material has no shear-coupling effect when the inclination angle is zero.

Influence of Collagen Orientation

The previous description about the structure of tendons is parallel. However, the anisotropy of the angular distribution of collagen fibrils in a sheep tendon was investigated using 1H double-quantum filtered nuclear magnetic resonance signals:

Table 4. Material constants of each level with different orientation angles (MPa). Note: the orientation angle is between collagen molecule and tendon.

	Matrix	Molecule	Fibril	Fiber	Fascicle	Tendon
	Input	Input	Theo	Theo	Theo	Theo
			Orientation angle 30°			
E_1	1[42]	3536	682	155	54	24
E_2	1[42]	53.2	36.2	24.6	17.0	12.0
μ_{12}	0.25	3.16	1.29	0.79	0.65	0.57
G_{12}	0.4	22.3	15.8	12.1	9.8	8.4
			Orientation angle 60°			
E_1	1[42]	3536	226	50	21	12
E_2	1[42]	53.2	35.9	25.1	20.8	23.8
μ_{12}	0.25	3.16	0.79	0.57	0.44	0.29
G_{12}	0.4	22.3	17.6	17.4	15.5	8.4
			Orientation angle 90°			
E_1	1[42]	3536	114	30	17	12
E_2	1[42]	53.2	35.8	30.2	53.8	750
μ_{12}	0.25	3.16	0.65	0.44	0.20	0.05
G_{12}	0.4	22.3	20.8	22.5	9.8	5

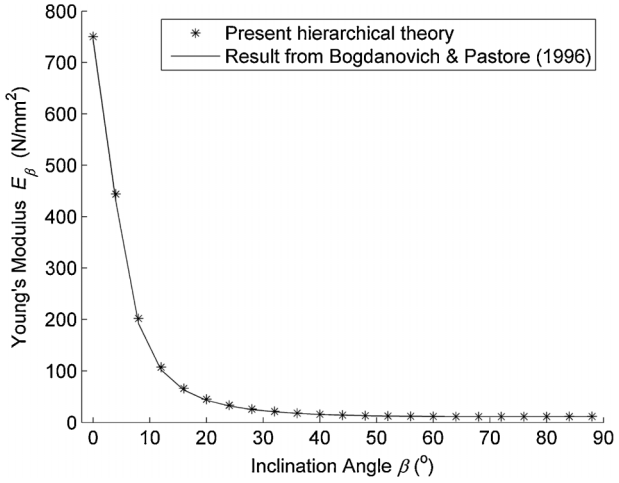

Fig. 15. Comparison between hierarchical theory and literature.

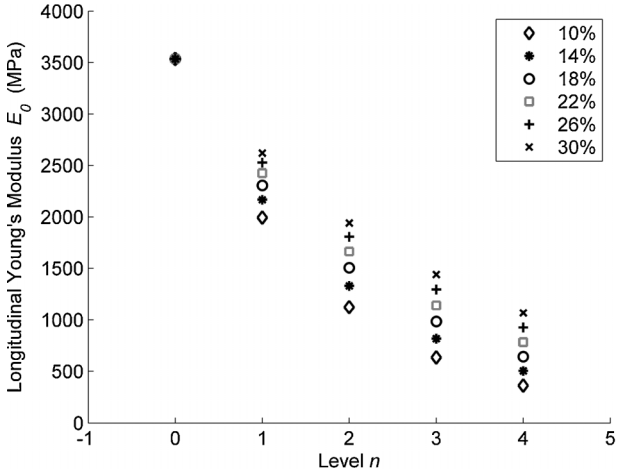

Fig. 16. Comparison between different volumetric fractions.

the angular distribution of collagen fibrils around the symmetric axis of the tendon was measured by the anisotropy of the residual dipolar couplings and described by a Gaussian function with a standard deviation of $12^\circ \pm 1^\circ$and with the center of the distribution at $4 \pm 1^\circ$.[51]

Accordingly, here, we change $\beta^{(i)}$ with 7.5° increment from 0° to 22.5°. Meanwhile, the included angle made by collagen molecule and tendon is $4\beta^{(i)}$, i.e., in the range 0–90°. The predictions are listed in Table 4. The hierarchical prediction of the Young's modulus is plotted in Figure 15 and compared with a different approach from the literature.[35] Figure 15 shows that the result determined by a different approach is slightly lower than that determined by our hierarchical theory.

Influence of the Total Volume of Collagen

The volumetric fraction of the collagen molecule is another important parameter influencing the material constants. Here, the elastic constants of the collagen molecule, reported in Table 2, are employed to investigate its influence when it varies in the range 10–30%, with 4% increment at each hierarchical level, see Figure 16. The result demonstrates that the elastic constants increase as the total volume of collagen increases.

Experiments on the Aechmea aquilegia Leaf

Experimental Procedure

In order to investigate the relationship between material constants and fiber orientation, we carried out ad hoc tensile tests employing a MTS micro-tensile machine. A leaf of the

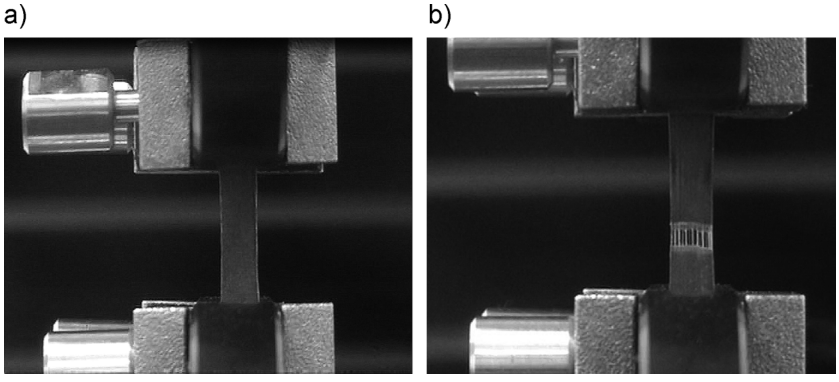

Fig. 17. Experimental process: (a) loading before failure and (b) failure with yield of emerging fibers.

Table 5. Experimental results on the tested leaves.

Angle (°)	0	10	20	30	40	50	60	70	80	90
Peak stress (MPa)	11.3 ± 0.1	8.9 ± 0.1	6.8 ± 1.5	4.8 ± 0.7	3.2 ± 0.9	3.7 ± 0.3	2.0 ± 0.5	2.6 ± 0.4	2.8 ± 0.3	2.1 ± 0.6
Peak Strain (mm mm^{-1})	0.17 ± 0.00	0.21 ± 0.00	0.19 ± 0.03	0.18 ± 0.02	0.16 ± 0.05	0.17 ± 0.05	0.12 ± 0.04	0.15 ± 0.06	0.20 ± 0.01	0.12 ± 0.03
Young's modulus (MPa)	127.0 ± 3.5	87.2 ± 7.2	62.1 ± 4.4	47.8 ± 4.4	29.3 ± 2.2	31.2 ± 3.7	18.5 ± 1.9	21.3 ± 3.0	16.4 ± 1.9	18.7 ± 0.3

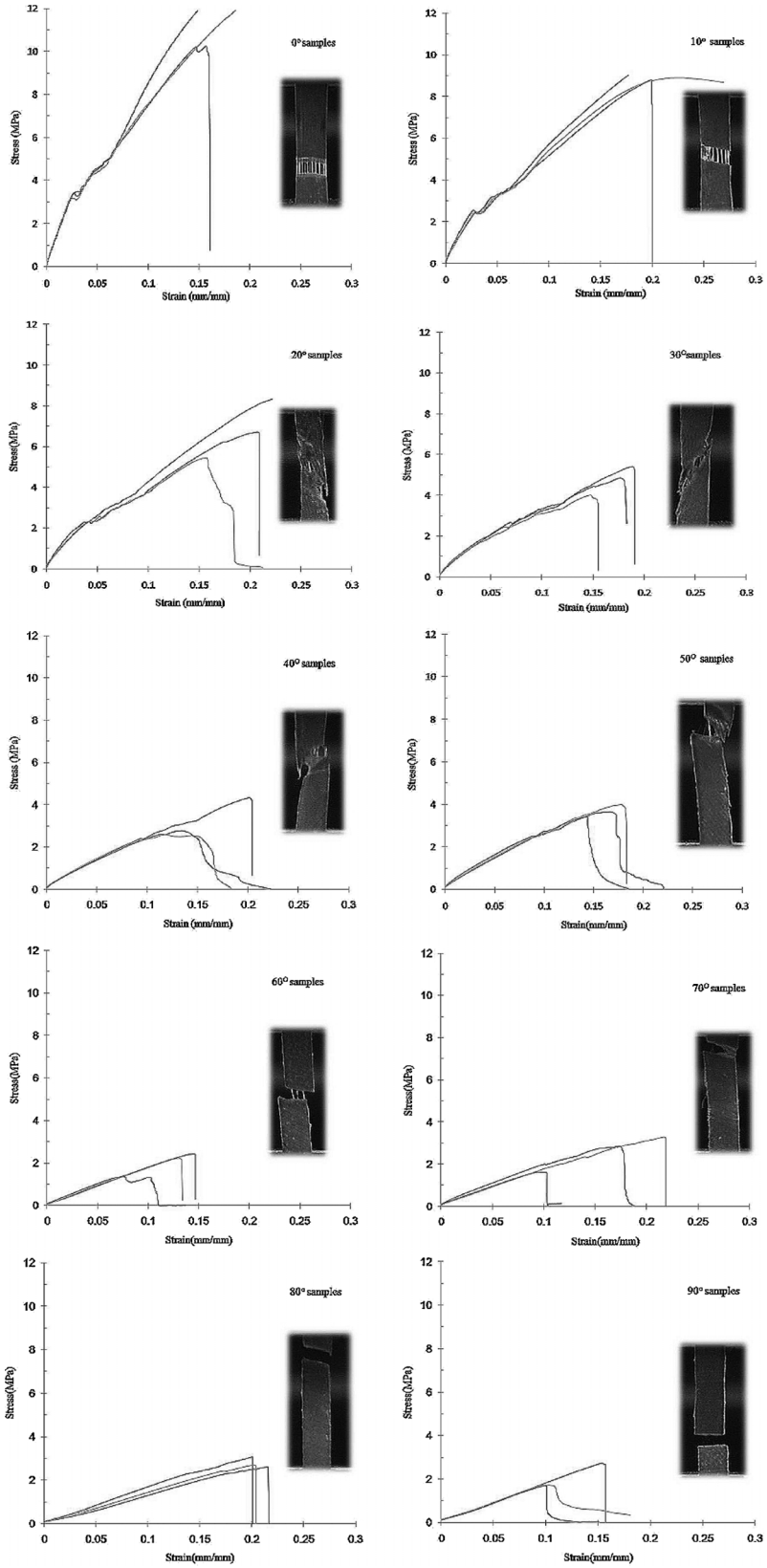

Fig. 18. Stress–strain curves and crack opening for the different tests.

Aechmea aquilegia was cut into 30 specimens with dimension $30\,\text{mm} \times 3\,\text{mm} \times 0.4\,\text{mm}$ on 1st December 2009; fiber inclination angles vary from 0° to 90° with 10° increment. The whole process was displacement controlled with a loading speed $1\,\text{mm}\,\text{min}^{-1}$ (Fig. 17(a) and (b)). All specimens were tested in indoor environment on 2nd December 2009. 12 days later (i.e., 14 December 2009), specimens were examined under SEM (Fig. 2).

Experimental Results and Discussion

The results of peak stress (or strength), peak strain, and Young's modulus are listed in Table 5.

The stress–strain curves are plotted in Figure 18. It suggests that, generally, peak stress (or peak load) and slope of each curve (or elastic modulus) decrease as the orientation (inclination angle) increases, while, the strain is always in the range of 0.15–0.20. Note that for the orientation angle $\beta^{(2)} \geq 70^\circ$, a bifurcation takes place: the crack path is not perpendicular to the loading direction but parallel to the fibers.

Prediction of the Hierarchical Theory

The analysis is based on the orthotropic material assumption for the leaf specimens. First, the five fitting parameters listed below are obtained by the experimental data of Young's modulus in Table 5: $E_f = 121.8\,\text{MPa}$; $E_m = 19.3\,\text{MPa}$; $\mu_{12} = 0.26$; $\mu_{21} = 0.04$; $G = 10.9\,\text{MPa}$.

Due to the direct SEM experimental observations (Fig. 2) and the schematic of the crack mouths (Fig. 17(b)), a hierarchical model, in which parts A,B,C,D are corresponding to those respectively appearing in Figure 2(a)–(d), is built (Fig. 19). The matrix is assumed to be isotropic with $E_m = 19.3\,\text{MPa}$ and $\mu = 0.25$, thus, the shear modulus is 7.72 MPa. The volumetric fraction $v_f^{(2)}$ is calculated from SEM observations, as $\approx 26.5\%$. In addition, $\beta^{(1)}$ is assumed to be 0° and $\beta^{(2)}$ depends on the specimens' inclination angle.

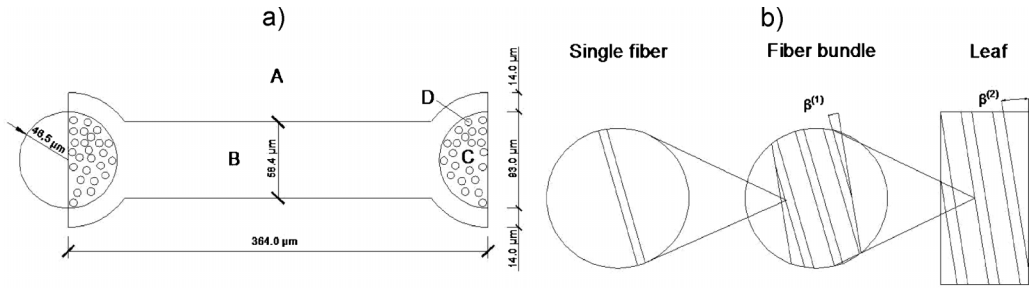

Fig. 19. Hierarchical model of the leaf: (a) cross-section and (b) hierarchical fibers.

Table 6. Material constants at each hierarchical level (MPa). Note: Theoretical predictions of fiber bundles do not change because $\mathbf{v}_f^{(2)} = \text{const.}$

(0°)	Matrix Input	Fiber Theo	Fiber bundle Theo	Leaf Input
E1	19.3	449–986	406	121.8
E2	19.3	10.4–16.0	16.5	19.3
μ12	0.25	0.3–0.43	0.29	0.26
G12	7.72	21.1–37.7	19.7	10.9

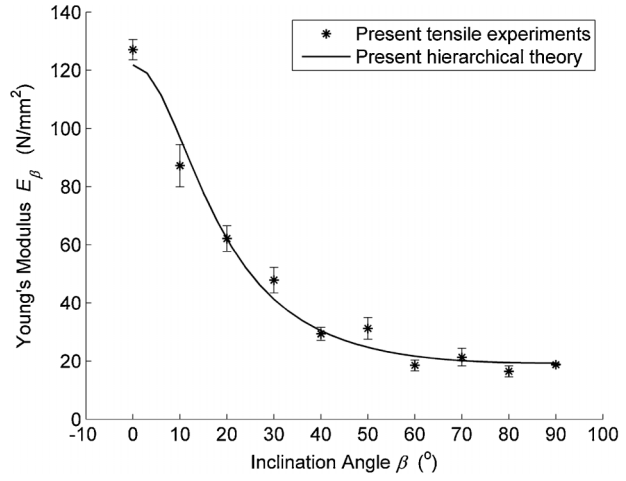

Fig. 20. Comparison between theoretical prediction and experimental data.

Inserting values of $v_f^{(i)}$ and $\beta^{(i)}$ into Equation 38, we have:

$$\begin{cases} [Q]^{(1)} = v_f^{(1)} \cdot [T(0)]^{-1}[Q]^{(0)}[T(0)] + \left(1 - v_f^{(1)}\right)[Q]_M \\ [Q]^{(2)} = 0.265 v_f^{(1)} \cdot \left[T\left(\beta_f^{(2)}\right)\right]^{-1}[Q]^{(0)}\left[T\left(\beta_f^{(2)}\right)\right] \\ \qquad + \left(1 - 0.265 v_f^{(1)}\right)[Q]_M \end{cases}$$

where, $[Q]^{(0)}$, $[Q]^{(1)}$, $[Q]^{(2)}$, and $[Q]_M$ are elastic matrices for fiber, fiber bundle, leaf, and matrix, respectively.

Herein, $v_f^{(1)}$ is selected in the range 0.4–0.9, and thus, the volumetric fraction $(v_f^{(1)} v_f^{(2)})$ is deduced in the interval 0.11–0.24. Finally, under the condition of $\beta^{(2)} = 0°$, the material constants of the leaf and matrix are given in Table 6.

Considering the material constants of a single fiber with $v_f^{(i)} = 0.9$, the Young's moduli of leaf for different inclination angles are compared with our theory in Figure 20, showing a relevant agreement.

Conclusions

We have developed a new theory for describing the elasticity of hierarchical tissues. The method stated in this paper shows the possibility of better understanding the elastic properties of biological materials or designing bio-inspired hierarchical tissues with desired elastic properties. In particular, the results show the possibility of designing a new class of hierarchical 2-D scaffolds by tailoring the elastic anisotropy, better matching the anisotropy of the biological tissues and thus maximizing the regeneration at each hierarchical level. The experimental results on tendons and leafs show a relevant agreement with the predictions of the proposed hierarchical theory.

Received: November 29, 2010
Final Version: February 16, 2011
Published online: April 21, 2011

[1] F. T. Moutos, L. E. Freed, F. Guilaka, *Nat. Mater.* **2007**, *6*, 162.
[2] S. C. Cowin, S. B. Doty, *Tissue Mechanics*, Springer, New York, USA **2007**.
[3] E. Baer, A. Hiltner, R. Morgan, *Phys. Today* **1992**, *45*, 60.
[4] N. Pugno, *Nanotechnology* **2006**, *17*, 5480.
[5] N. Pugno, A. Carpinteri, *Phil. Mag. Lett.* **2008**, *88*, 397.
[6] N. Pugno, F. Bosia, A. Carpinteri, *Small* **2008**, *4*, 1044.
[7] N. Pugno, *Mater. Today* **2010**, *13*, 40.
[8] M. A. J. Cox, N. J. B. Driessen, R. A. Boerboom, C. V. C. Bouten, F. P. T. Baaijens, *J. Biomech.* **2008**, *41*, 422.
[9] P. X. Ma, *Mater. Today* **2004**, *7*, 30.
[10] C. Liu, Z. Xia, J. T. Czernuszka, *Chem. Eng. Res. Des.* **2007**, *85*, 1051.
[11] S. J. Hollister, *Nat. Mater.* **2005**, *4*, 518.
[12] M. J. Buehler, Y. Yung, *Nat. Mater.* **2009**, *8*, 175.
[13] R. Ritchie, M. J. Buehler, P. Hansma, *Phys. Today* **2009**, *62*, 41.
[14] M. J. Buehler, S. Y. Wong, *Biophysics* **2007**, *93*, 37.
[15] M. J. Buehler, *PNAS* **2006**, *103*, 12285.
[16] M. J. Buehler, *Nanotechnol. Today* **2010**, *5*, 379.
[17] M. J. Buehler, *Nat. Nanotechnol.* **2010**, *5*, 172.

[18] Z. Q. Zhang, Y. W. Zhang, H. Gao, *Proc. R. Soc. B* **2011**, *278*, 519.
[19] H. Tang, M. J. Buehler, B. Moran, *Ann. Biomed. Eng.* **2009**, *37*, 1117.
[20] F. H. Silver, J. W. Freeman, G. P. Seehra, *J. Biomech.* **2003**, *36*, 1529.
[21] L. Yang, Mechanical properties of collagen fibrils and elastic fibers explored by AFM, PhD Thesis **2008**.
[22] N. Sasaki, S. Odajima, *J. Biomech.* **1996**, *29*, 655.
[23] N. Sasaki, S. Odajima, *J. Biomech.* **1996**, *29*, 1131.
[24] L. Bozec, M. Horton, *Biophys. J.* **2005**, *88*, 4223.
[25] J. A. J. Van der Rijt, K. O. Van der Werf, M. L. Bennink, P. J. Dijkstra, F. J. Jan, *Macromol. Biosci.* **2006**, *6*, 697.
[26] L. Yang, C. F. C. Fitie′, K. O. Van der Werf, M. L. Benninkb, P. J. Dijkstra, F. J. Jan, *Biomaterrials* **2008**, *29*, 955.
[27] L. Z. Yin, D. M. Elliott, *J. Biomech.* **2004**, *37*, 907.
[28] R. M. N. Arib, S. M. Sapuan, M. M. H. M. Ahmad, M. T. Paridah, H. M. D. Khairul Zaman, *Mater. Design* **2006**, *27*, 391.
[29] L. U. Devi, S. S. Bhagawan, S. Thomas, *J. Appl. Polym. Sci.* **1998**, *64*, 1739.
[30] J. George, S. S. Bhagawan, N. Prabhakaran, S. Thomas, *J. Appl. Polym. Sci.* **1995**, *57*, 843.
[31] S. Mishra, A. K. Mohanty, L. T. Drzal, M. Misra, G. Hinrichsen, *Macromol. Mater. Eng.* **2004**, *289*, 955.
[32] R. M. Christensen, *Mechanics of Composite Materials*, John Wiley & Sons, New York, USA **1979**.
[33] T. Fu, J. Zhao, K. Xu, *Mater. Lett.* **2007**, *61*, 330.
[34] R. F. Gibson, *Principles of Composite Material Mechanics*, first ed. (Eds: J. J. Corrigan, E. Castellano), McGraw-Hill, New York, USA **1994**.
[35] A. Bogdanovich, C. Pastore, *Mechanics of Textile and Laminated Composites*, first ed. Chapman & Hall, London, UK **1996**.
[36] S. K. Lee, J. H. Byun, S. H. Hong, *Mater. Sci. Eng.* **2003**, *347*, 346.
[37] T. M. Mcbride, J. L. Chen, *Compos. Sci. Technol.* **1997**, *57*, 345.
[38] R. Lakes, *Nature* **1993**, *361*, 511.
[39] V. C. Mow, A. Radcliffe, S. L.-Y. Woo, *Biomechanics of Diarthroidal Joints*, first ed. Springer, New York, USA **1990**.
[40] R. M. V. Pidaparti, A. Chandran, Y. Takano, C. H. Turner, *J. Biomech.* **1996**, *29*, 909.
[41] M. Paulsson, P. D. Yurchenco, G. C. Ruben, J. Engel, R. Timpl, *J. Mol. Biol.* **1987**, *197*, 297.
[42] M. Lavagnino, S. P. Arnoczky, E. Kepich, O. Caballero, R. C. Haut, *Biomech. Model. Mech.* **2008**, *7*, 405.
[43] Y. P. Kato, D. L. Christiansen, R. A. Hahn, S. J. Shieh, J. D. Goldstein, F. H. Silver, *Biomaterials* **1989**, *10*, 38.
[44] S. P. Magnusson, M. Hansen, H. Langberg, B. Miller, B. Haraldsson, E. K. Westh, S. Koskinen, P. Aagaard, M. Kjaer, *Int. J. Exp. Pathol.* **2007**, *88*, 237.
[45] R. R. Lemos, M. Epstein, W. Herzog, *Med. Biol. Eng. Comput.* **2008**, *46*, 23.
[46] M. Ito, Y. Kawakami, Y. Ichinose, S. Fukashiro, T. Fukunaga, *J. Appl. Physiol.* **1998**, *85*, 1230.
[47] G. A. Lichtwark, A. M. Wilson, *J. Exp. Biol.* **2005**, *208*, 4715.
[48] K. M. Quapp, J. A. Weiss, *Biomech. Eng.* **1998**, *120*, 757.
[49] H. A. Lynch, W. Johannessen, J. P. Wu, A. Jawa, D. M. Elliott, *J. Biomech. Eng.* **2003**, *125*, 726.
[50] S. H. Scott, G. E. Loeb, *J. Morphol.* **1995**, *224*, 73.
[51] R. Fechete, D. E. Demco, B. Blumich, U. Eliav, G. Navon, *J. Magn. Reson.* **2003**, *162*, 166.

